GIS-Based Landslide Susceptibility Modeling Using Frequency Ratio and Logistic Regression at Abuna Gindeberet area, West Shewa Zone, Central Ethiopia

Migartu Abdissa Tukku

A Thesis Submitted To the Department of Applied Geology

School of Applied Natural Science

Presented in Partial Fulfillment of the Requirement for the Degree of Master's in Engineering Geology

Office of Graduate Studies

Adama Science and Technology University

October, 2023

Adama, Ethiopia

GIS-Based Landslide Susceptibility Modeling Using Frequency Ratio and Logistic Regression at Abuna Gindeberet area, West Shewa Zone, Central Ethiopia

Migartu Abdissa Tukku

Advisor: Matebie Meten (PhD)

A Thesis Submitted To the Department of Applied Geology

School of Applied Natural Science

Presented in Partial Fulfillment of the Requirement for the Degree of Master's in Engineering Geology

Office of Graduate Studies

Adama Science and Technology University

October, 2023

Adama, Ethiopia

DECLARATION

I hereby declare that this Master Thesis entitled "GIS-Based Landslide Susceptibility Modeling Using Frequency Ratio and Logistic Regression at Abuna Gindeberet area, West Shewa Zone, Central Ethiopia" is my original work. That is, it has not been submitted for the award of any academic degree, diploma or certificate in any other university. All sources of materials that are used for this thesis have been duly acknowledged through citation

Migartu Abdissa Tukku	________________________	________________
Name of the student	Signature	Date

RECOMMENDATION

We, the advisors of this thesis, hereby certify that We have read the revised version of the thesis entitled “GIS-Based Landslide Susceptibility Modeling Using Frequency Ratio and Logistic Regression at Abuna Gindeberet area, West Shewa Zone, Central Ethiopia” prepared under our guidance by **Migartu Abdissa Tukku** submitted in partial fulfillment of the requirements for the degree of Mater’s of Science in **Engineering Geology.** Therefore, we recommend the submission of revised version of the thesis to the department following the applicable procedures.

Matebie Meten (PhD)	____________________	________________________
Major Advisor	Signature	Date
Shankar Karuppannan (PhD)	________________________	________________
Co-advisor	Signature	Date

APPROVAL PAGE

We, the advisors of the thesis entitled "GIS-Based Landslide Susceptibility Modeling Using Frequency Ratio and Logistic Regression at Abuna Gindeberet area, West Shewa Zone, Central Ethiopia" and developed by Migartu Abdissa Tukku, hereby certify that the recommendation and suggestions made by the board of examiners are appropriately incorporated into the final version of the thesis.

Matebie Meten (PhD)	____________________	____________________
Major Advisor	Signature	Date
Shankar Karuppannan (PhD)	____________________	______________
Co-advisor	Signature	Date

We, the undersigned, members of the Board of Examiners of the thesis by Migartu Abdissa Tukku have read and evaluated the thesis entitled "GIS-Based Landslide Susceptibility Modeling Using Frequency Ratio and Logistic Regression at Abuna Gindeberet area, West Shewa Zone, Central Ethiopia" and examined the candidate during open defense. This is, therefore, to certify that the thesis is accepted for partial fulfillment of the requirement of the degree of Master of Science in Engineering Geology.

Pradeep Kamaraj (PhD)	____________________	____________________
Chairperson	Signature	Date
Yadeta Chemdesa (PhD)	____________________	____________________
Internal Examiner	Signature	Date
Leulalem Shano (PhD)	____________________	____________________
External Examiner	Signature	Date

Final approval and acceptance of the thesis is contingent upon submission of its final copy to the Office of Postgraduate Studies (OPGS) through the Department Graduate Council (DGC) and School Graduate Committee (SGC).

________________________	____________________	____________________
Department Head	Signature	Date
________________________	____________________	____________________
School Dean	Signature	Date
________________________	____________________	____________________
Office of Postgraduate Studies, Dean	Signature	Date

ACKNOWLEDGMENT

Above all; I thank God for his sympathy, kindness, and grace throughout my life. My sincere respect and special thanks go to Dr. Matebie Meten and Dr. Shankar Karuppanan for their initiation and for providing excellent advice and constructive comments. Words could not express your dedication, guidance, encouragement, supervision, and scientific advice that have been decisive for the successful completion of this thesis.

I express my deep gratitude to Adama Science and Technology University for sponsoring and giving all facilities starting from the beginning of the courses until the completion of this study.

I also thank the National Meteorological Agency of Ethiopia (NMAE) for providing meteorological data, the Geological Survey of Ethiopia (GSE) for providing geological maps and the Ethiopian Space Science and Geospatial Institute for providing topographic maps of the study area.

Moreover, I'd like to thank my family for all the support and encouragement throughout the thesis work. Finally, I would like to thank all my friends for their motivation to do better work.

Table of Contents

Contents **Pages**

List of Figure

List of Table

Lists of plate

Plate Pages

List of Abbreviations and Acronyms

AUC	Area Under Curve
DEM	Digital Elevation Model
ESSGI	Ethiopian Space Science and Geospatial Institute
FR	Frequency Ratio
GIS	Geographical Information System
GSE	Geological Survey of Ethiopia
LSA	Landslide Susceptibility Analysis
LSI	Landslide Susceptibility Index
LSM	Landslide Susceptibility Map
LR	Logistic Regression
LULC	Land Use Land Cover
NMAE	National Metrological Agency of Ethiopia
ROC	Receiver Operating Characteristics
USGS	United States Geological Survey

ABSTRACT

Landslide is one of the greatest disasters that cause the damages to properties and loss of life. Landslide susceptibility mapping was carried out for the Abuna Gindeberet area of the West Shewa Zone in central Ethiopia. The main objective of this study is to prepare causative factors and landslide susceptibility maps using GIS-based frequency ratios and logistic regression models. Based on Google Earth imagery, about 1222 landslides were identified and classified randomly into training landslide datasets (70%) for model development and the remaining (30%) validation landslide datasets in the ArcGIS environment. The eight landslide causative factors like slope, aspect, curvature, lithology, land use/land cover, distance to lineament, distance to stream, and rainfall, were identified and integrated with training landslides to determine the weights of each factor class and landslide causative factors using frequency ratio and logistic regression models, respectively. The landslide susceptibility maps were produced by overlaying the weights of all the landslide causative factors using the raster calculator of the spatial analyst tool in ArcGIS 10.8. The final landslide susceptibility maps were reclassified as very low, low, moderate, high, and very high susceptibility classes in both frequency ratio and logistic regression models. The results of landslide susceptibility maps produced by the frequency ratio model indicate that the very low, low, moderate, high, and very high susceptibility classes cover 9%, 21%, 24%, 34%, and 12% of the area, respectively. Similarly, the landslide susceptibility maps produced from the logistic regression model revealed that 7%, 33%, 9%, 28%, and 23% of the area fall in the very low, low, moderate, high, and very high classes respectively. These susceptibility maps were validated by the receiver operating characteristic (ROC) of the area under the curve (AUC). The AUC results of the frequency ratio and logistic regression models showed success rates of 0.857 and 0.849, respectively, while the prediction rates for these models are 0.828 and 0.831, respectively. Thus, the landslide susceptibility map (LSM) using the validation dataset provided acceptable results, and the different classes that are delineated using these models can be used in the future for safe development planning in the study area.

Keywords: *Landslide, Causative Factors, GIS, Frequency Ratio, Logistic Regression, Susceptibility Maps*

1. INTRODUCTION

1.1 Background of the study

Landslides are one of the most frequent natural hazards, causing a lot of damage to property and infrastructure and loss of lives worldwide (Chandra and Indrajit, 2019; Li *et al*., 2021). Natural hazards such as landslides, floods, earthquakes, and drought risk cannot be avoided completely, but the processes and consequences can be mitigated. Landslides are more widespread than any other geological event; and can occur anywhere in the world. They occurred due to conditioning and triggering factors (Getachew and Meten, 2021).

Landslides occur when the driving force exceeds the resisting force; as a result, the natural soil or rock slopes will become unstable. Both natural and man-made factors such as improper land use, loss of sediment, prolonged and heavy rain, highly weathered and fractured rocks, gully and riverbank erosion, earthquakes due to superficial soil-rock interference, and unplanned urban expansion will destabilize the natural slope (Woldearegay, 2013; Wubalem and Meten, 2020). Due to the complex geomorphological, environmental, hydrological, and geological setting, active geodynamic process, and unplanned land use practice, the landslide activities in Ethiopia are primarily linked with the northern, northwestern, central, southern and southwestern rift escarpments.

Landslides in Ethiopia have resulted in the loss of human and animal lives; and damaged infrastructures and properties in the last five decades (Woldearegay, 2013; Meten *et al*., 2015; Wubalem and Meten, 2020; Berhane and Tadesse, 2021; Beza, 2021; Genene and Meten, 2021; Shano *et al*., 2021; Wubalem, 2021). The occurrence of landslides is an extremely complex phenomenon that depends upon various factors such as geologic structure, lithological association, topography, rainfall, earthquake, and human activity (Mandal, 2018).

The current study area is found at Abuna Gindeberet District, West Shewa Zone, Oromia Regional State in Central Ethiopia. Due to the recent occurrence of numerous active landslides that significantly damaged farmlands, houses, and gravel roads, this area is highly susceptible to landslide problems. The vulnerability of people's lives and property to landslides requires special attention, and the area has not yet been studied.

Therefore, proper investigation is needed in this area to determine the types, causes, and failure mechanisms of landslides and to develop landslide susceptibility maps showing where landslides are most likely to occur.

One of the most widely used approaches to the landslide distribution but not to reduce the landslide damage is preparing a landslide susceptibility mapping using suitable models and selecting the effective conditioning factors (Anis *et al*., 2019). Over the last decades, many studies have used different models to prepare landslide susceptibility maps. These models include the frequency ratio model (Shano *et al*., 2021) and, Weights of evidence model (Getachew and Meten, 2021). Landslide susceptibility models based on the bivariate frequency and Weights of evidence models (Mersha and Meten, 2020) and frequency ratio and information value models (Genene and Meten, 2021; Wubalem, 2021). Landslide susceptibility models based on the bivariate frequency ratio and multivariate logistic regression models (Prakash, 2015) were applied in a GIS environment. Geographical Information System (GIS) platforms help to calculate and visualize the cumulative effects of conditioning factors on landslide occurrence.

However, each of the above-mentioned methods has certain limitation in terms of landslides susceptibility mapping, which may produce various conditions. Therefore, the combination of bivariate FR and multivariate LR statistical models was used in this study to tackle the limitation of using only bivariate or multivariate methods. Therefore, the study applied the FR and LR models in a GIS environment to produce the landslide susceptibility maps, which help to identify the highly susceptible areas and the most critical conditioning factors responsible for landslide occurrence in the study area. Therefore, it is vital to utilize the various landslide susceptibility mapping techniques so as to evaluate and delineate landslide-prone areas for proper and strategic land use planning.

1.2 Statement of the Problem

Landslides/slope instability problems occur every rainy season in the Ethiopian highlands. Several published or unpublished investigations using analytical, qualitative, or empirical methods have previously been conducted in various regions of the Ethiopian Highlands (Ayalew, 1999; Ayalew and Yamagishi, 2004; Ayenew and Barbieri, 2005; Raghuvanshi et al., 2014). The current study area was situated in the central Ethiopian highlands of Abuna Gindeberet district in the west shewa zone of the Oromia region.

In recent years, there have been a number of landslide occurrences in the study area. Residents in this area have lost their homes and farmland, forcing them to leave. No landside study has been conducted in the current study area. This study will be undertaken to increase the awareness of residents, decision-makers, and scholars about landslide-related problems in this area. For this purpose, the area's landslide susceptibility maps (LSM) were prepared using frequency ratio and logistic regression models.

1.3 Objectives

1.3.1 General Objectives

The general objective of the study is to evaluate the causative factors and model the landslide of the study area using GIS-based frequency ratio and logistic regression models.

1.3.2 Specific objective

The specific objectives of this study are aimed at:

- Prepare a landslide inventory map of the study area.
- Prepare the landslide causative factor maps for this study.
- Identify which factor classes and factor maps significantly contribute to landslide occurrences.

1.4 Significance of the Study

Abuna Gindeberet area is frequently affected by landslide problems. A landslide susceptibility map is useful for land use planning, natural risk management, and developing mitigation measures. In this study, landslide susceptibility maps were prepared, which are used for planners with a practical and effective way to identify and delineate the landslide-prone areas.

Moreover, it is crucial to enhance safety and adopt strategic planning for future developmental activities like selecting suitable sites for agriculture, settlements, and other developmental initiatives. Additionally, providing relevant information to local, zonal, regional, and federal governments regarding current and prospective land use practices can prove invaluable in mitigating the forthcoming impacts of landslides in vulnerable areas.

1.5 Scope of the study

The investigation was conducted in Abuna Gindeberet District, including Bukato, Dokonu Sure, Goho Guduru, Dogsa Goro, Mukarba, Insilale, and Mudi Ula Kara villages in West Shewa Zone of central Ethiopia to prepare landslide susceptibility maps using frequency ratio and logistic regression models in a GIS environment.

1.6 Limitation

Finding time series images that show when and how the landslide occurred in the study area was challenging, and the situation concerning landslide disaster preparedness and environmental safety is worrying. Another notable limitation in this study was the absence of crucial causative factor maps, ideally at or below a scale of 1:50,000. Specifically, the unavailability of key maps of the lithological map. Additionally, the discontinuous record of rainfall stations from the NMAE data introduced further constraints in this study.

2. LITERATURE REVIEW

2.1 Landslide

Landslides are the most destructive geological hazards worldwide, threatening both human beings and property (Lee, 2019). Landslides are signs of slope instabilities, defined as the tendency for a slope to undergo morphologically and structurally disruptive landslide processes. They could be manifested individually and in combinations of various forms, including the emergence of springs, seeps, or saturated ground in areas that have not typically been wet before, new cracks or unusual bulges in the ground, street pavements, or sidewalks, soil slide away from foundations, tilting of ancillary structures from the main house, cracking of concrete floors, structures and walls, disrupted drainage ditches, leaning telephone or electric poles, trees, retaining walls or fences, offset fence lines, sunken or down-dropped road beds, bulging and cracking of the ground, sudden decrease in stream water level while under rain are all surface manifestations indicating emergence of landslides (Rotaru, 2007). However, landslides/slope failures are not as costly as earthquakes, major floods, hurricanes, or some other natural catastrophes.

2.2 Landslide Studies in Ethiopia

Despite the challenge’s landslide research in the country, and various study reports of different time have shown the actuality and destructiveness of landslides in the highland of Ethiopia. For instance, authors like Woldearegay (2008) and Girma et al. (2015) reported the occurrence of landslides in the highlands of Ethiopia. Research revealed that most slope failures prevailed in these areas with certain geological (lithological and structural) settings, slope shapes, slope gradients, drainage lines (stream incisions/gullying), artificial excavations (cuts), and vegetation cover. Woldearegay (2013a) stated that the complex geomorphological, hydrological, and geological setting of the hilly terrains of the Ethiopian landmass made this area highly susceptible to frequent landslides. The general physiography of the Ethiopian Highlands is controlling landslide occurrences in Ethiopia.

2.2.1 Landslide in the Northern Highlands of Ethiopia

Landslide in the northern highlands of Ethiopia, particularly in Dessie town, is the most highly researched area by different authors in different periods. Ayenew (2002) and Ayenew and Barebieri (2005) are among the authors who reported the landslides in Dessie town.

The study from these authors generalized that; the slope failure involved unconsolidated materials which overlie the trap volcanic. Accordingly, a number of mitigation measures have been implemented, but despite these efforts, landslides still remain major challenges for the development of Dessie town. In conclusion, many researchers participated in landslide-related problems of the Dessie town in the northern highland of Ethiopia. This implies the attention given to understanding the damage and devastation-caused by this natural hazard. Recently, Ayalew et al. (2009) mentioned the challenges of the on-going road rehabilitation works in the area.

2.2.2. Landslide in the Central and South Western Highlands of Ethiopia

Different scholars stated that landslides are the causes of the damage to properties and human life (Meten, 2015; Meten et al., 2015; Prakash, 2015). Meten et al. (2015) reported that only from 1960 to 2010, about 388 people were dead, 24 people were injured, and plenty of agricultural lands, houses, and infrastructures were affected.

Prakash (2015) reported that more than 3000 people were displaced, and the landslide damaged 1250 dwelling houses. In addition, one church, one elementary school, and four-grain mills were completely destroyed in the Tarmaber landslide (Woldearegay, 2008). The landslide also devastated about 1,500 hectares of agricultural land and damaged the natural environment significantly.

Zerihun Dawit (2016) reported that a landslide had killed 51 people from 2005 to 2016 in the Kindo Didaye district in south west highlands of Ethiopia in which prolonged rainfall was considered as an external triggering factor of the event besides relief, slope geometry, structural discontinuity, land use and groundwater-surface manifestations as intrinsic causes.

Broothaerts et al. (2012) reported the occurrence of a landslide in Gilgel Gibe catchment in south west Ethiopia. This study indicated that deforestation and heavy rainfall were the main conditioning and triggering factors, respectively, to cause the removal of 1 million cubic slope materials. Tsige et al. (2017) found that landslides and associated ground subsidence damaged to the major infrastructures in Bonga Town. The author concluded that the presence of heavy rainfall coupled with the construction activity, which avoided water drainage and changes in groundwater level, was the main cause of the problem.

2.3. Landslide Causative Factors

The conditions that increase landslide susceptibility without actually causing one and tend to keep the slope in a moderately stable state are known as landslide regulating factors (Woldearegay, 2013). The processes and factors that affect slope stability are vast and diverse; and interact in complex ways (Woldearegay, 2008). For this reason, different scholars' classifications of the components will vary. For instance, Carrara and Pike (2008) classified these components as conditioning and triggering factors.

Cruden and Varnes (1996) further divided the causes of slope failure into geological, hydrological, and human activity. I.e. (lithology and distance from fault as geological factors), (rainfall, drainage network as hydrological), (slope, curvature, elevation, aspect as topographic), and human causes (change in land use and cover).

2.3.1. Geological Factors

The geological features are known as landslide occurrences in various ways. Lithology and fault are examples of geological factors. Hard and massive rocks resist erosion since each geological unit has its own lithological characteristics (Anbalagan and Singh, 2001).

According to Hadmoko et al. (2010), locations near fault lines are more likely to be exposed to slope material displacement than areas farther away. According to Woldearegay (2005), the prevalence of landslides in areas underlain by Paleozoic glacial, Post-glacial sediments, and shale (in northern Ethiopia) is attributed to the fact that these slope masses are associated with: (a) low shear strength behaviors, (b) low permeability characteristics which enhance the development of seepage forces within the overlying slope masses, and (c) high susceptibility to weathering, erosion, and lubrication (softening). A similar observation was reported by Ayalew and Yamagishi (2004) on the landslide problems in the Abay gorge. The authors indicated that overlain by loose soil masses and/or intercalated within more resistant rocks, shale materials are important factors affecting slope stability.

2.3.3. Topographic Factors

Various variables are categorized under topographic factors that influence slope failure including elevation, aspect, curvature and slope (Cruden and Varnes, 1996).

2.3.3.1 Slope

Gravity is known to be the common force drives movement on slopes. A review of the previous studies showed that most of the reported debris/earth slides/flows and rockslides have occurred place in areas with slope angles between 15 and 45 degrees. As indicated by different researchers (Mersha and Meten, 2020; Wubalem and Meten, 2020; Genene and Meten, 2021) reported that slope angles greater than 12 degrees may have a high probability of landslide occurrence. The low landslide probability of occurrence in low slope gradients is due to an increase in the factor of safety, and thus, a higher water table will be required to initiate failure (Ayalew and Yamagish, 2004; Ayenew and Barbieri, 2005; Woldearegay, 2005).

2.3.3.1 Curvature

Slope curvature influences the susceptibility of a slope to landslide by governing the distribution of water (surface/subsurface) within a slope. Positive plan curvature values (convex) indicate the divergence and negative plan curvature values (concave) indicate the water concentration. Concave plan terrains promote water concentration, while convex plan terrains cause flow divergence. Ayalew and Yamagishi (2004) and Woldearegay (2005) indicated that many landslides have occurred in concave areas, with some on planar terrains. According to these authors, the high susceptibility of concave areas to rainfall-triggered landslides is related to the fact that such terrains are associated with the (a) convergent water flows (surface and subsurface), which leads to water pressure build-up, (b) high susceptibility to subsurface erosion (piping), due to concentrated subsurface water flow along pervious layers, and (c) greater thickness of unconsolidated deposits as these areas are generally zones of material accumulation.

2.3.4. Human Induced Factors

Human-induced factors are variables that can influence the occurrence of mass wasting due to human activity. Road constructions in hilly or mountainous areas are examples of anthropologically induced slope instability (Ayalew and Yamagishi, 2005). A similar study also showed landslide occurrence in cut and-fills (roadway and building excavations), river bluff failures, lateral spreading landslides, and a wide variety of slope failures associated with quarries. From hydrological perspective, road segments may act as the barrier, sink, or corridor of water flow that affects slope stability. Sideng et al. (2018) indicated that human activities such as constructing roads, cutting slopes and clearing land could be triggering factors of landslides.

In general, the slope instability is controlled by external (triggering) and internal (conditioning) factors. The only difference seen during this review was the way words are used among different authors. Therefore, similar concepts but different approaches and methods were considered based on the topography and geological variability in the local area. As indicated above, the influencing factors such as topographical, geological, and human-induced factors were the most general factors that control the slope instability. These factors are responsible for the historical and present landslide occurrences, which can affect the future landslide occurrence probability in similar conditions (Guzzetti *et al*., 2005).

2.4. Landslide Susceptibility Analysis Methods

These landslide susceptibility analysis techniques can be classified as expert (qualitative), and quantitative (statistical and deterministic) approaches (Fall et al., 2006). According to van Westen et al. (2006), landslide inventory-based probabilistic methods are the most widely produced outputs. The author also argues that the past landslide events are good indicators of the likelihood of the phenomena in the future under the same geo-environmental conditions. Therefore, using a landslide inventory map helps derive information on the historical event for the future prediction of landslide occurrence.

According to most literature, the commonly adopted approach for landslide susceptibility analysis can be divided into qualitative and quantitative (Fall et al., 2006; Sashikant, 2009). Qualitative methods are very subjective as well as site-specific, and up-scaling to a larger area is a problem. On the other hand, the quantitative methods provide numerical estimations in terms of the probability of landslide spatial occurrences. This approach uses the relation between the locations of previous landslide events and environmental variables to predict areas of landslide initiation with a combination of factors.

In reviewing various literatures, the quantitative method can further be partitioned in to heuristic and statistical. The statistical methods have become important in recent years and are preferred over the heuristic methods as they are independent of expert bias and purely quantitative (van Westen et al., 2006). Chung and Fabbri (2003) recommended the flexibility and objectivity of statistical methods in predicting landslide susceptibility by using statistical models and remotely sensed data. Besides, Guzzetti et al. (2005) and Leta (2007) used a landslide inventory map to drive data for landslide quantification, which can only be achieved using a statistical approach. Faus (2011) also combined the statistical and heuristic methods for future slope failure estimation in Karanganyar Regency – Indonesia, concluding that the statistical method is more consistent than the heuristic one.

2.4.1. Statistical Analysis Techniques

These methods are applied based on statistical analysis of a group of causative variables in a particular location. These are indirect ways, and the landslide hazard strategy is based on a statistically evolved rule with the relative contributions of each causative parameter (Carrara *et al*., 1992). Statistical methods can be bivariate and multivariate (Dai and Lee, 2001).

2.4.1.1 Bivariate Statistical Method

This technique is one kind of statistical approach. In order to determine the relative contribution of each factor class in initiating a landslide, individual factor maps are overlaid on a historical landslide inventory map. To determine the landslide susceptibility, weights are computed for each factor class. Based on the density of the landslides, weights are assigned to each causative factor. This method includes various statistical techniques like information value, frequency ratio, weight of evidence, weighted overlay, fuzzy logic, certainty factor, statistical index, and density area methods (Kanungo et al., 2009). These bivariate statistical techniques were developed for landslide susceptibility mapping.

2.4.1.1.1 Frequency Ratio Methods

The frequency ratio approach is based on relationships between the distribution of landslides and each factor associated with landslides to correlate between the locations of landslides and the factors associated with landslides in the study area (Lee and Pradhan, 2007). To calculate the frequency ratio, the area ratio of landslide occurrence and non-occurrence was calculated for different classes or types of each factor, after which an area ratio for the class or type of each factor of the total area was calculated.

$$\text{Frequency Ratio (FR)} = \frac{\text{Slide Ratio}}{\text{Class Ratio}} \qquad (1)$$

$$\text{Slide Ratio} = \frac{\text{Number of landslide pixel in class}}{\text{Total number of landslide pixel}} \qquad (2)$$

$$\text{Class Ratio} = \frac{\text{Number of pixel in individual class}}{\text{Total number of pixel in whole class}} \quad (3)$$

The FR value represents degree of the correlation between landslides and the concerned class of the conditioning factors. So, a value of 1 means an average value. If the value is > 1, there is a high correlation, and FR < 1 means a lower correlation. Then, the landslide susceptibility index (LSI) was calculated in spatial analysis tools of raster calculator by adding FR values of all causative factors.

$$LSI = \sum FR = FR1 + FR2 +. . + FRn. \quad (4)$$

2.4.1.2 Multivariate Statistical Method

A multivariate statistical model forecasts the spatial occurrence of landslides. This method takes into consideration the relative contribution of each thematic data layer to the total landslide susceptibility (Ayalew and Yamagishi, 2005; Kanungo et al., 2009; Shano et al., 2020).

The logistic regression method and discriminant method, including artificial intelligence methods, artificial neural network method, support vector machines, probabilistic approach, and deterministic approach, are among the common methods for landslide susceptibility/hazard analysis (Shano et al., 2020). As Prakash (2015) and Wubalem and Meten (2020) indicated, logistic regression is the most popular multivariate statistical analysis model that can be used to establish a multivariate regression relationship between dependent and independent variables.

2.4.1.2.1 Logistic Regression

The most popular multivariate technique is logistic regression, as it can be used to forecast a result measured by a binary variable, such as the presence or absence of landslides based on a set of one or more independent variables, and the independent variables do not need to have a normal distribution as the independent variables can be non-linear, continuous, categorical or a combination of continuous and categorical (Prakash, 2015). The main objective is finding the model in logistic regression that best explains how a dependent variable and a group of independent variables are best related (Ayalew and Yamagishi, 2005). The logistic regression model has emerged as one of the most reliable statistical tools for mapping landslide vulnerability and identifying the key factors influencing landslides (Wubalem and Meten, 2020).

The relationship between the occurrence and its dependence on various variables can be quantified as follows.

$$p = \frac{1}{(1+e^{-z})} \qquad (5)$$

Here, P is the estimated probability of landslide occurrence, which varies from 0 to 1 on an S-shaped curve, and Z is the linear combination. The spatial databases of each factor were saved in dbf format files for use in the statistical package, and the correlation between landslide and all factors was calculated.

$$z = b_0 + b_1x_1 + b_2x_2 + b_3x_3 + b_4x_4 + b_5x_5 + b_nx_n \qquad (6)$$

Where b_1, b_2, b_3 … b_n are logistic regression coefficients of the factors, x_1, x_2, x_3 … x_n are factors and b_0 is the intercept.

These equations can be used to generate a map of the area's landslide susceptibility by calculating the probability that predicted the possibility of a landslide.

3. METHODS AND MATERIALS

3.1 Description of the study area

The study area is located in the Abuna Gindeberet District of the West Shewa Zone of the Oromia Region of Central Ethiopia. It is located 176 Km west of the capital city (Addis Ababa). It is bordered by Meta Robi district in the East, Gindeberet district in the West, Jeldu district in the South, and Amhara Regional State in the North. The area is located between 9°26'N and $9^0$50'N latitude and $37^0$50'E and 38°10'E longitudes. The elevation ranges between 1068m up to 2593m m above sea level (Figure 1). This area can be classified into two main physiographic regions: - plateau area and rugged terrain. The area is highly susceptible to active surface processes because of the presence of sharp ridges, cliffs, rugged slope faces, steep scarps, deep gorges, and valleys.

The study area is vegetated, with eucalyptus trees, wild grass, and sporadic bushes covering most ridges. Most of the study area is gently sloping terrain and flat land, which are heavily used for agriculture and grazing land. Teff, Sorghum, Barley, Wheat, Beans, maize and pulses are the most widely grown agricultural crops.

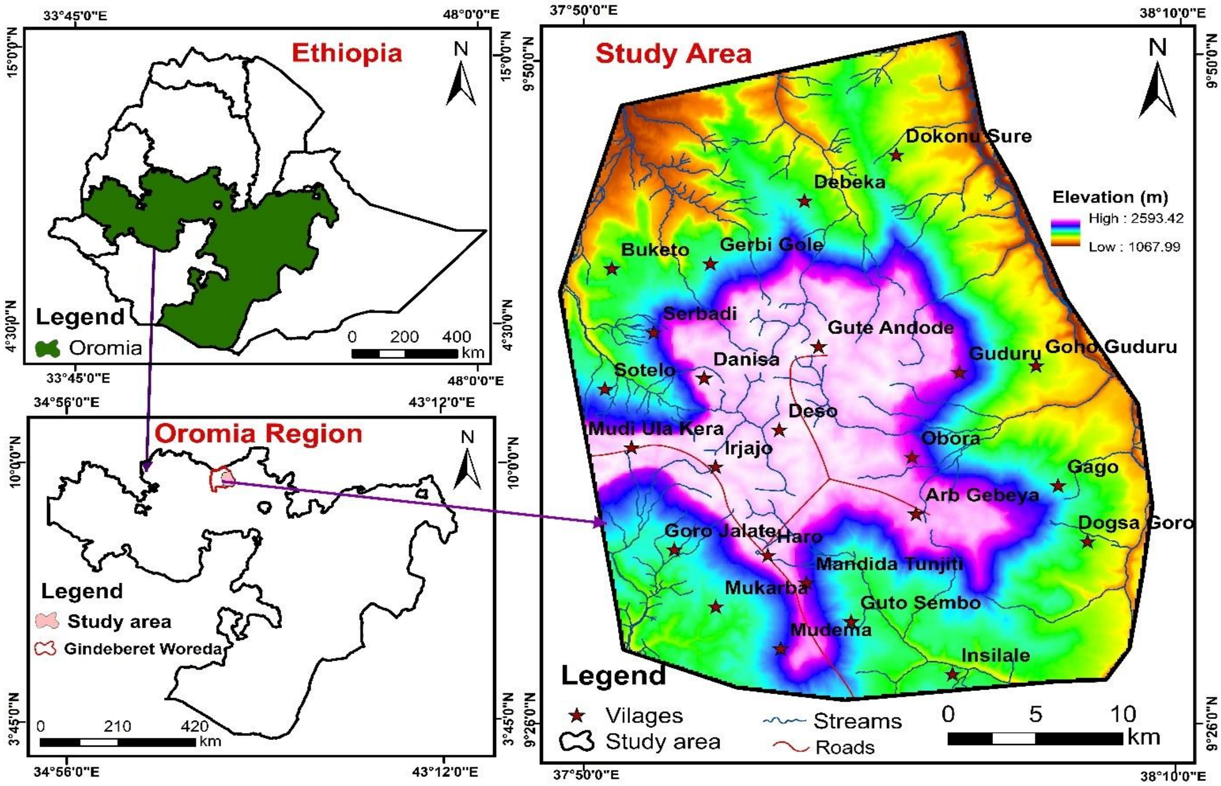

Figure 1Study area location map

Climate conditions

The climatic condition of the area showed that the wet season starts in May and extends up to October, and the peak wettest season occurs in July and August with a maximum monthly rainfall of 350mm and 450mm, respectively (Figure 2a). This area receives rainfall twice a year, with heavy precipitation from June to September and light to moderate precipitation from mid-March to mid-April. The main rainy season is from June to the end of September. Appendix I indicates the rainfall data for all stations given by the National Meteorological Agency of Ethiopia.

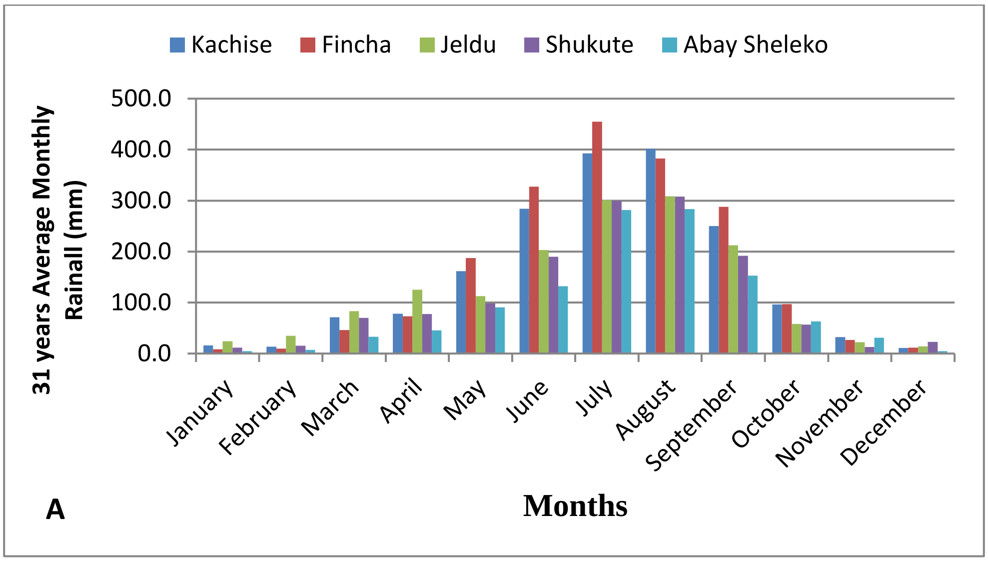

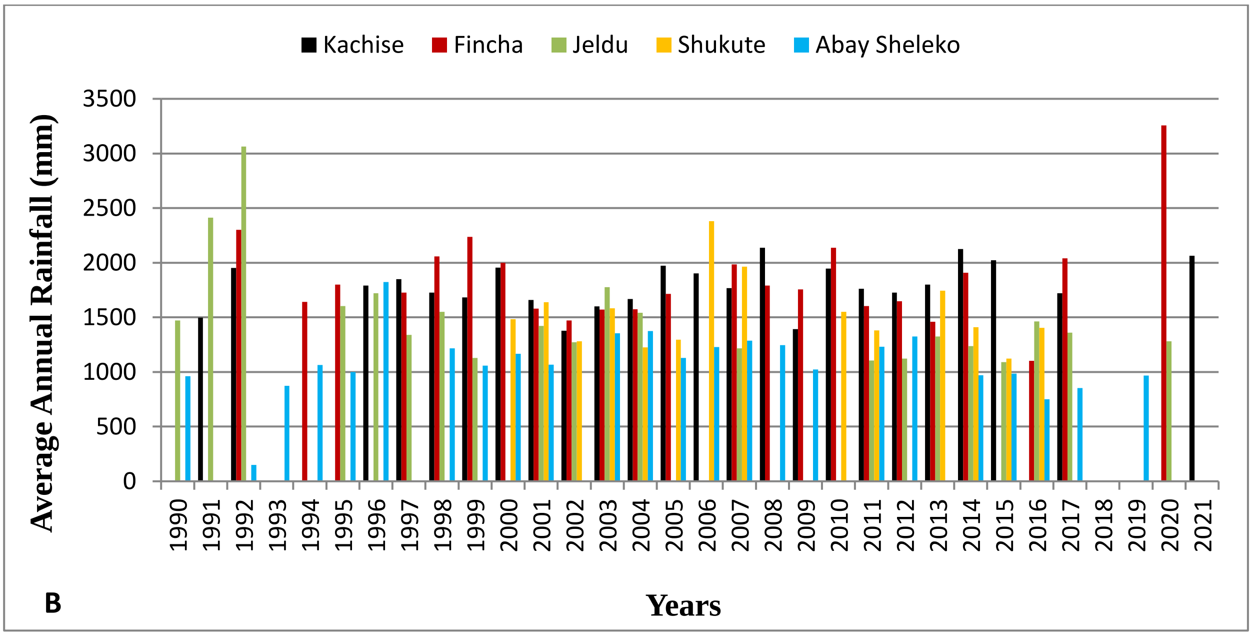

Figure 2 A) Average monthly rainfall, B) average annual rainfall of the study area

3.2 Data Sources

This part involved the collection of spatial and non-spatial data from primary and secondary sources.

Table 1 Data type and sources

Types of Data	Sources	Purpose
Published and unpublished papers	Google scholar	To have a general background and a conceptual framework for the study
Topographic map	ESSGI	To digitize streams, roads, and villages
Geological maps	GSE	Digitized Lithology
Meteorological data	NMAE	Rain-fall Map
DEM	USGS	To generate slope, aspect and curvature
Google Earth Image	Google earth pro	To identify the landslide inventory, land use/land cover, and Lineament

3.3 Materials and Software Used

3.3.1 Materials

The different types of materials which are used in these stages are laptop, topographic map, and stationery supplies, including note-book, pen, and pencil. From the beginning to the end of this study, various activities were accomplished and drawn using a laptop, and stationery materials were performed.

3.3.2 Software's

Microsoft Office Word 2010 and Microsoft Office Excel 2010 were used for data handling and report writing. ArcGIS version 10.8.1 was used to prepare different thematic maps. SPSS software was used for logistic regression and ROC analysis, and Google earth pro was used to prepare the landslide inventory, land use/land cover, and lineament maps.

3.4 Data Collection

3.4.1. Primary Data

In order to prepare the landslide inventory map, a high-quality Google earth image was used. The data was used for validating the causative factor maps and landslide inventory maps for the areas. Thus, Google earth pro image was used to generate primary landslide inventory data.

The following tasks were carried out during the investigation phase:

- Relevant information about the locations, modes of failure, and sizes of previous landslides was gathered from Google Earth Pro.
- The land use/land cover map was generated from Google Earth Pro.
- Lineaments were identified from Google Earth Pro.

3.4.2 Secondary Data

Secondary data were collected from different institutions/organizations, including a literature review on both published and unpublished papers from different online and journal sources, a topographic map from the Ethiopian Space Science and Geospatial Institute, regional geological map from the Geological Institute of Ethiopia and metrological data from National Meteorological Agency of Ethiopia.

3.5 Landslide Susceptibility mapping

For landslide susceptibility mapping, existing landslides are used to evaluate the possible areas of future landslides. The bivariate and multivariate statistical approaches are used to analyze the spatial distribution of landslides in the landslide susceptibility maps. Bivariate statistical analyses perform an individual statistical assessment of each factor in relation to landslide occurrence. Several bivariate (information value, weights of evidence, certainty factor function, and frequency ratio) approaches were developed for landslide susceptibility mapping (Pradhan, 2007). Multivariate statistical models like logistic regression method, artificial intelligence methods, artificial neural network method, support vector machines, probabilistic approach, and deterministic approach are used to forecast spatial landslide occurrence (Shano et al., 2020). This study used the bivariate statistical approach (frequency ration) and multivariate statistical approach (logistic regression) models.

3.5.1 Landslide susceptibility mapping using frequency ratio method

The frequency ratio approach is based on the observed relationships between the distribution of landslides and each landslide-related factor to reveal the correlation between landslide location and the factors in the study area (Lee and Pradhan, 2007). In order to evaluate the relationships between the causative factors and landslide distribution, each causative factor was reclassified, and landslides were overlaid over each factor map to determine the frequency ratio values of all the classes of each factor map (equation 2 and 3) in ArcGIS.

The frequency ratio values for each landslide factor were tabulated and graphically plotted in a Microsoft Excel spreadsheet based on equation 1. Then, the frequency ratio values of each factor map class were assigned in ArcGIS, and finally, the frequency ratio of all the factor maps was added to the raster calculator of the spatial analysis tools to produce the landslide susceptibility index (equation 4) and the landslide susceptibility index was reclassified in to five landslide susceptibility classes.

3.5.2 Landslide susceptibility mapping using the Logistic regression Method

Logistic regression is one of the several multivariate analysis techniques. Statistically, elements can be categorized into one of the two populations using logistic regression. In this instance, a unit of analysis (pixel) and the populations of landslide occurrence or nonoccurrence cases would be more appropriate replacements for the term's elements and populations, respectively. This implies a comparison and correlation between the variance of data sets from specific populations considered the independent variable and the variance of data from the dependent variable. Again, in this case, the dependent variable represents the occurrence/non- occurrence of landslide cases, while the independent variables represent the causative factors. Then, the landslide inventory training data set was classified into landslide points and non-landslide points in ArcGIS. Landslide point and non-landslide point of training data sets were extracted with the frequency ratio of each causative factor and imported to the SPSS statistical package in dbf format. Through SPSS, the logistic regression coefficients of each factor and constant were computed, and linear combinations were computed in the raster calculator of spatial analysis tools. The final landslide susceptibility map was computed in the 3D analyst tool of ArcGIS based on equation (5) and reclassified in to five susceptibility classes.

3.6 Landslide inventory data

Landslide inventories are essentially factual in nature (Fell et al., 2008). As Corominas and Mavrouli (2023), landslide inventory data is highly important for producing a reliable map that predicts the landslide susceptibility maps in a certain area. It is crucial to have insight into landslides' spatial and temporal frequency. The landslide inventory map was digitized from high-resolution tracking using Handheld GPS through field surveying where the area is accessible to identify landslides and digitized from Google earth for inaccessible landslide areas like gorges, valleys, high cliffs, and river banks. This study digitized the landslide inventory map from Google earth image interpretation.

The landslide inventory map is the most important data source as it contains information on the locations where landslides have actually taken place. Landslide information should be stored with the type of landslide, the state of activity, and, if possible, the date of occurrence and damage caused (Corominas and Mavrouli, 2023).

Landslide inventories are the basic analysis and recording of landslides that applies the basic principle in which ‘‘the past is the key to the future’’ (Aipe and Sailesh, 2016). It should give insight into the location, date, type, size, activity and causal factors of landslides as well as the resulting damage.

3.7 Data Analysis

Data was analyzed based on primary and secondary data as the following procedures:

- The landslide inventory polygon was created from a Google Earth image.
- For land use/land cover map preparation, the Google earth image of 2023 was used, which was re-digitized and rasterized in ArcGIS10.8.1.
- Thematic map layers of causative factors were prepared using secondary and primary data in ArcGIS10.8.1. Then, all these maps were transformed into raster format with the same cell size of 30 by 30m.
- Raster Calculator calculated landslide susceptibility index maps for frequency ratio and probability values for logistic regression models in ArcGIS.
- Finally, five landslide susceptibility classes with very low, low, moderate, high, and very high classes were prepared for both frequency ratio and logistic regression models.
- In the end, landslide susceptibility maps were validated through the validation landslide inventory map, and the predictive and success rates were compared using AUC and ROC values.

3.8 Methods

In order to achieve the objectives of this study, the following procedures were followed.

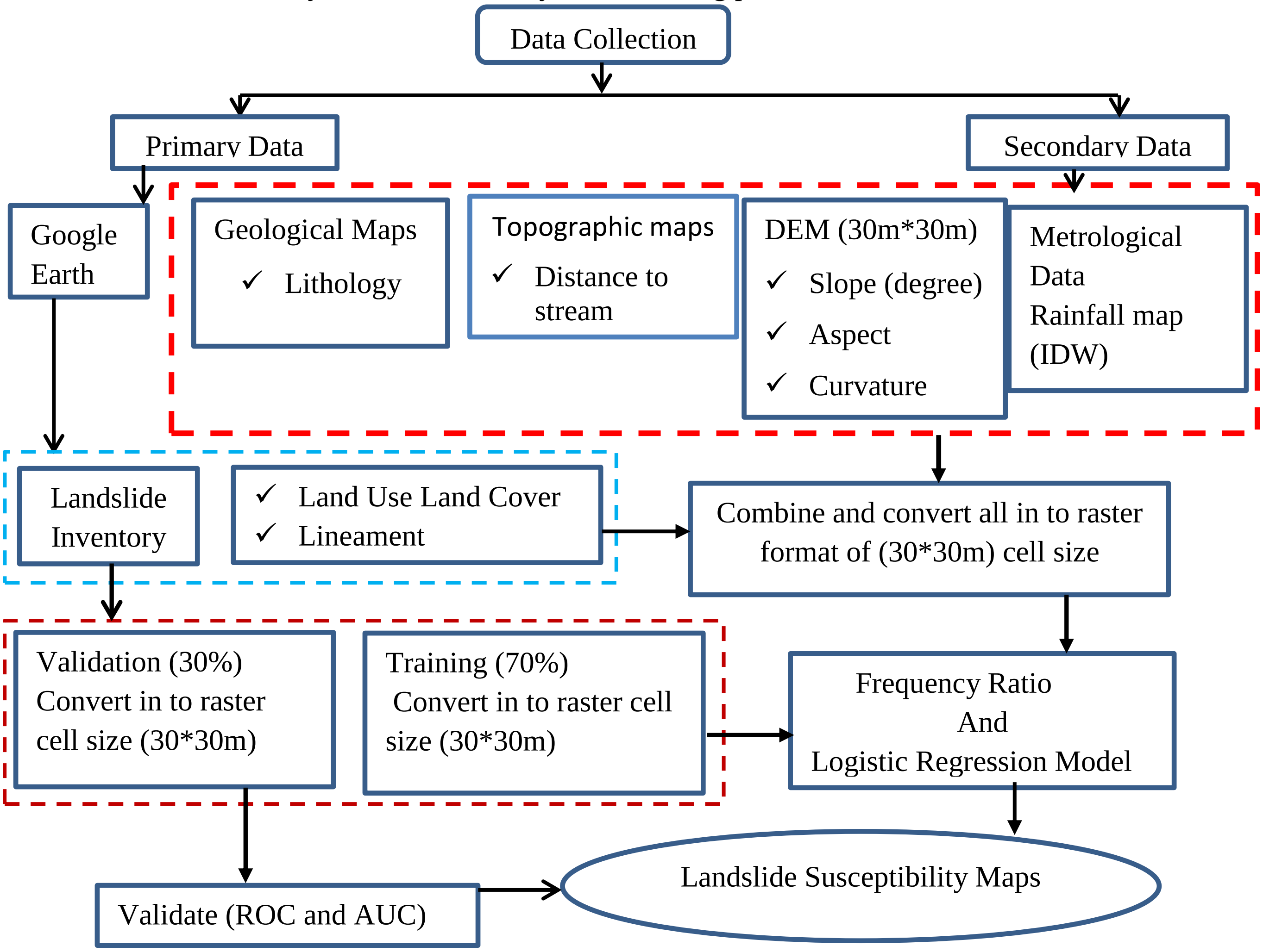

Figure 3 Overall methodological flow chart

4. GEOLOGY

4.1 Regional Geology

The current study area is found in Ethiopia's Blue Nile Basin, one of the major East African sedimentary basins. Ethiopia's sedimentary regions cover a significant portion of the country's surface (Beyth, 1972). They are divided into five separate basins: the Ogaden, Abbay, Gambela, Southern Rift, and Mekele basins (Assefa, 1991). These five basins cover 33% of Ethiopia's surface (Ahmed, 2008). Among these basins, the northwest sedimentary basin occupies the majority of the country and is characterized by highlands that range in altitude from 1500 to 4000 m, while the southeast plateau, which the Ogaden Basin occupies, is relatively low in elevation and descends to the Indian Ocean (Asefa, 1991). According to Ayalew and Yamagishi (2004), the history of Mesozoic sedimentation was connected to the start of Gondwanaland's break-up during the Paleozoic and Jurassic periods, which was predominantly governed by faults. Abay Gorge (Blue Nile Basin) formed during the intra-continental rift stage, which was associated with the start of Gondwanaland's break-up (Russo et al., 1994). According to Russo et al. (1994), the Tertiary flood basalt covers the Blue Nile River Basin, which is 1200 meters thick and is divided into five units from bottom to top: Antalo limestone - represents the result of a major transgression, muddy sandstone (Mugher sandstone) and upper sandstones (Debra Libanos Sandstone) - formed by regression of the sea from the main water body. Lower Sandstone (Adigrat Sandstone)- represents the post-rift deposition by fluvial sedimentation. These formations contain a variety of rock types, including sandstone cliffs that extend for distances, limestone that is interspersed with shale and marl, and gypsum that is mixed with relatively soft mudstone, shale, and marl units that are susceptible to mass movement (Asefa, 1981). The regional geological map of the study area, which was taken from the Geology of Addis Ababa Map Sheet of 1:250,000 scale, includes Quaternary Superficial Sediment, Middle and Lower Basalt, Antalo Limestone, Gohatsion formation, Adigrat Sandstone, pre-Adigrat Sandstone, Granite and Biotite-hornblend Gneiss.

4.2 Local geology

The study area is part of the Blue Nile basin containing seven lithological units such as Alluvial deposit, Quaternary superficial sediment and Residual soil, basalt, Limestone, Gohatsion Formation and Sandstone.

Table 2 Area coverage of each lithological unit

Lithology	Area (km^2)	Area (%)
Sandstone	303	33.6
Alluvial Soil	5	0.5
Limestone	210	23.3
Basalt	67	7.4
Gohatsion Formation	139	15.4
Quaternary Superficial Sediments	28	3.1
Residual Soil	149	16.6

Sandstone

This lithological unit covers a large area of the study, which accounts for 33.6% of the total area. This unit mainly forms a steep slope and is overlain conformably by limestone formation. It is exposed mostly around the boundary area.

Limestone

In the study area, this unit is overly on the sandstone unit and directly underlies the tertiary basalt. It contains limestone beds ranging in thickness from thin to thick. It has a light gray color, is highly weathered, and has a gentle slope towards a sharp contact with the Gohatsion Formation. Limestone is fine-grained and cover 23.3% of the study area (Table 2). Blanford first named it at the type locality as limestone in the Tigray region (1870).

Gohatsion formation

This unit is exposed mainly from the southern to northern parts of the study area map. It covers an area of 139 km^2 and 15.4% of total study area. The nature of contact with the overlying limestone and the underlying sandstone which is marked by a 20m thick multiple lamination, of shale and mudstone. In the study area, white friable Gohatsion is observed.

Basalt

This basalt overlies the limestone unit, and it covers 7.4% of the study area.

Alluvial deposits

Alluvial deposits are unconsolidated and weathered materials that occupy low-lying areas close to the river courses and streams and deeply cut gullies. It covers the smallest portion (0.5%) of the study area (Table 2). The alluvial deposit is thick and consists of unconsolidated silt, sand, pebbles, and cobble.

Residual Soil

Mostly, the plateau part of the study area is dominantly covered by this unit which is the result of weathering and decomposition of the underlying basaltic rock in its original place of formation. This indicated that this soil is extremely erodible and covers 16.6% of the area (Table 2).

Quaternary Superficial Sediment

This soil is deposited in some parts of the plateau area and mostly of alluvial soil, and it is light grey and dark gray in color. It covers the smallest portion (3.1%) of the study area (Table 2).

5. RESULT AND DISCUSSION

5.1 Landslide Inventory Map

From the finding of landslide inventory through Google earth image interpretation, a total of 1222 landslides were identified in the study area and mapped as vector-based polygons. Then by supporting ArcGIS, the vector data was converted to the raster format with a pixel size of 30m by 30m, and; they were randomly subdivided into two data sets: 70%, which is 855 landslides used for the susceptibility model building, and the remaining 30% of 367 landslides used for model validation. Landslides in the landslide inventory maps are mainly distributed in the study area's northern, west, and south parts, characterized by rugged and steep slopes, deep gorges, and highly fractured and weathered rocks. The landslides include debris slides, rotational and translational slides, rock slides, creep and earth slide types of landslides. All landslide events are represented by polygon features, which the landslide classification system developed by Varnes in 1978.

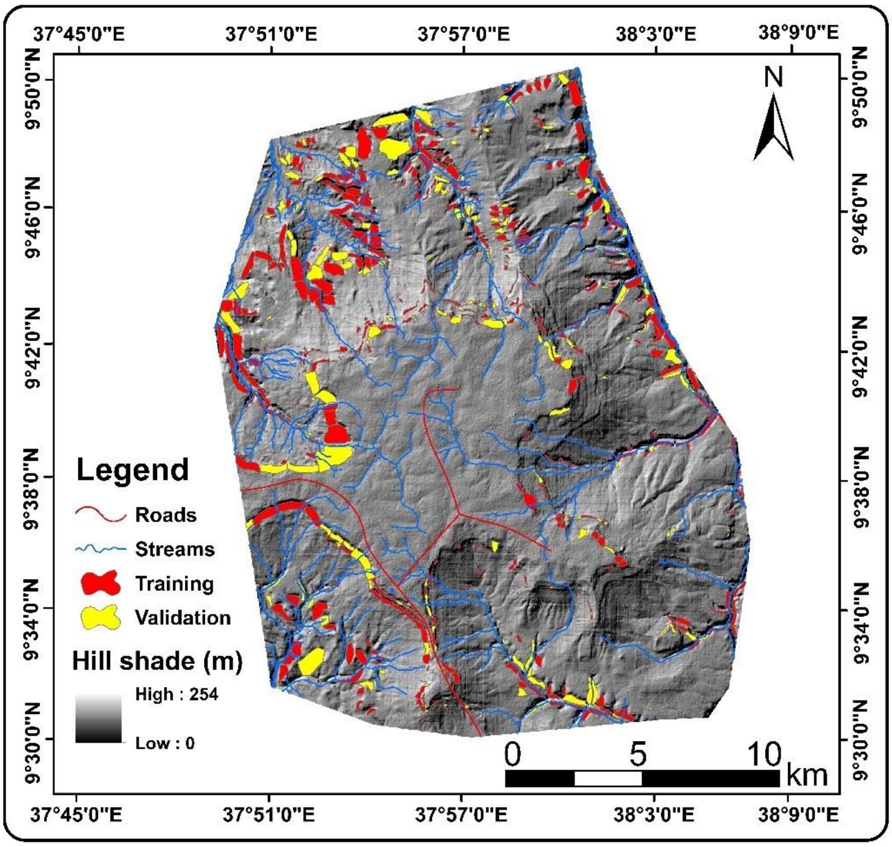

Figure 4 Landslide inventory map of the study

Plate 1-3 indicates some images of landslide inventory in the study area.

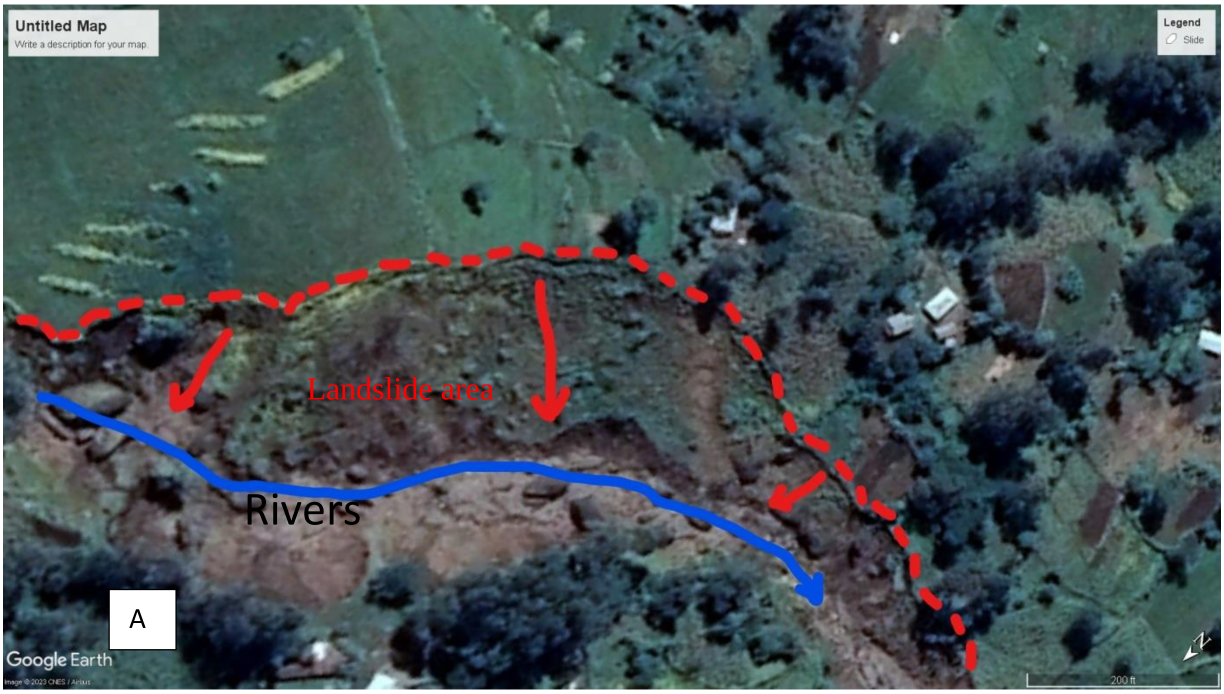

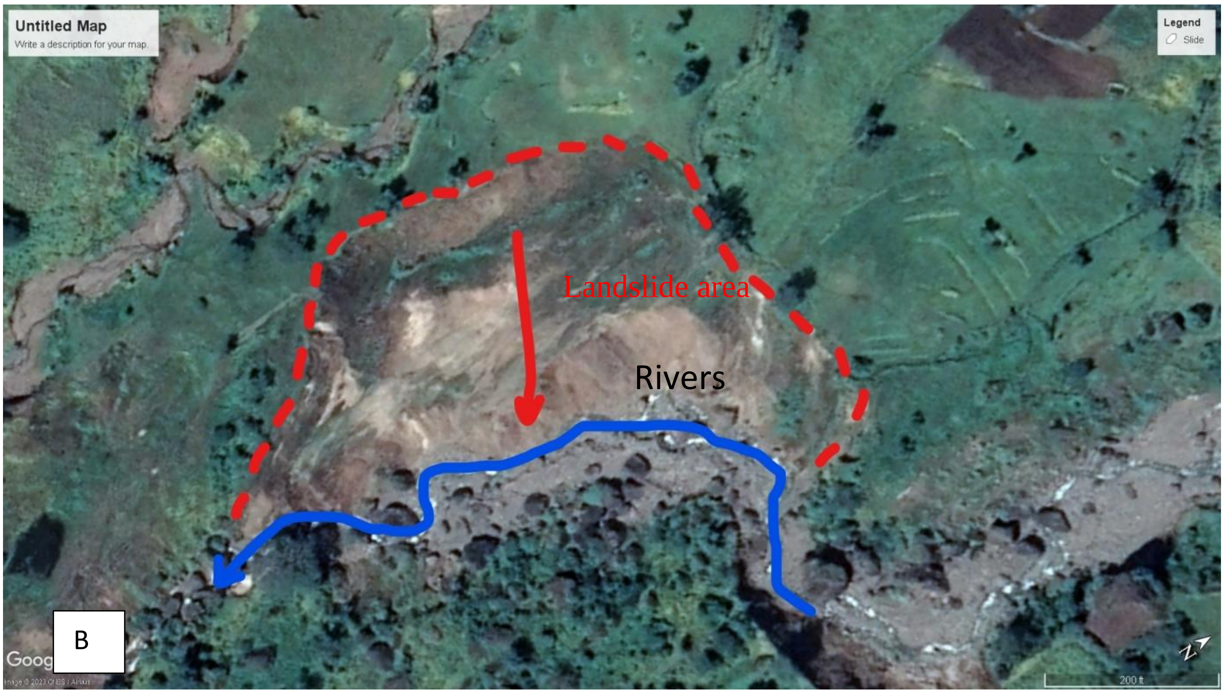

plate 1 Goro Jalate localities; a) creep, b) Earth slide, c) creep of stream under cut

As the plate indicated the large agricultural land of a localities affected due to stream under cutting and heavy rain fall.

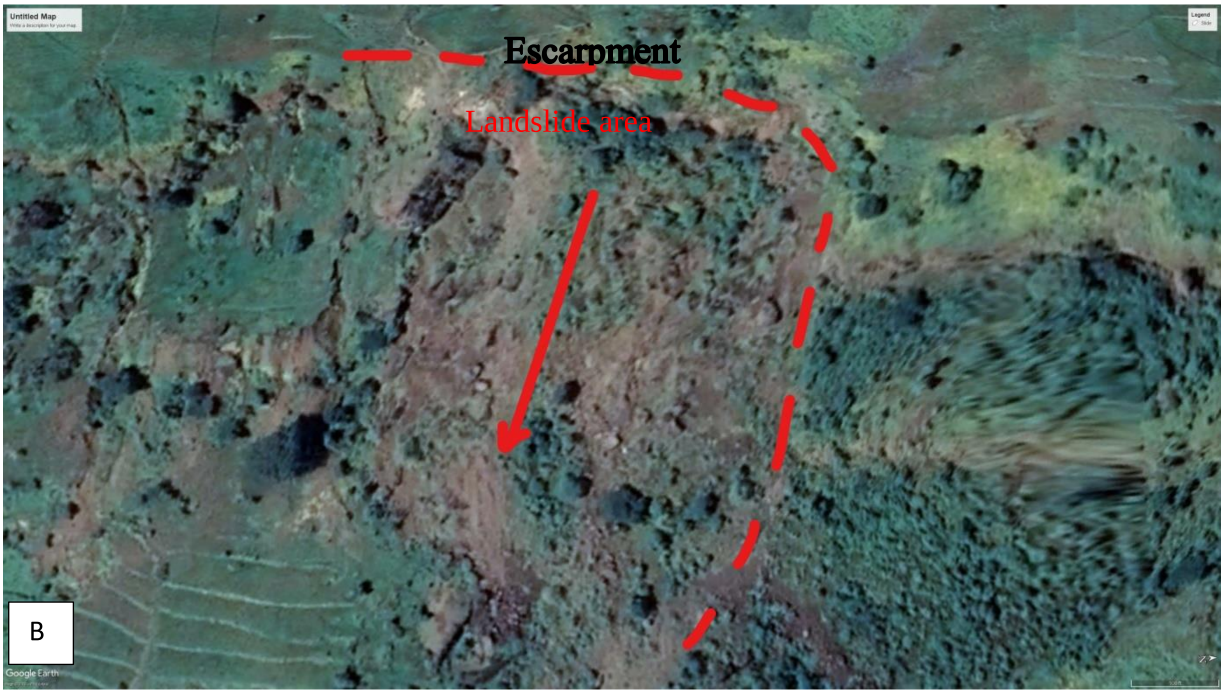

plate 2 Mudema localities a) Rock fall b) Rock slide along the escarpement

Mudema locality was located near the bottom of a highly and slightly weathered basalt forming a steep slope. As a result, large areas of agricultural land were affected, as shown on plate 2 above.

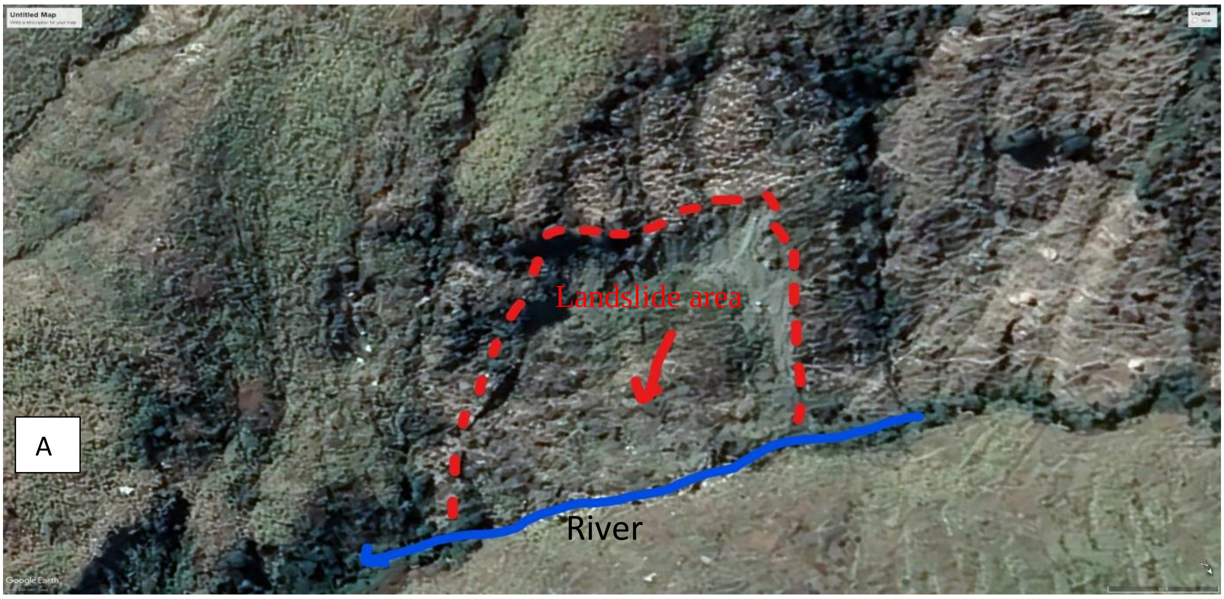

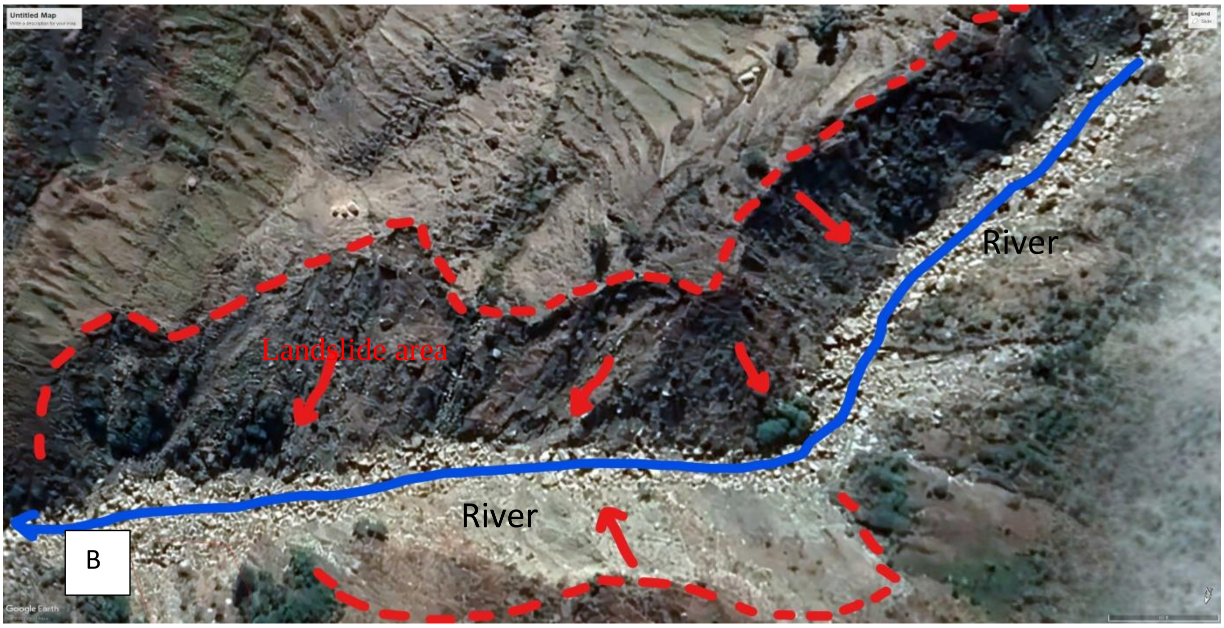

plate 3 A) Rock slide and B) earth slide at Guduru locality

5.2 Landslide Causative Factor maps

For landslide studies, it is assumed that a certain location could have a landslide as a result of a particular set of conditions relevant to numerous causative factors. According to studies by Chimidi et al. (2017), Girma et al. (2015), and Shano et al. (2020), the prediction of probable areas where future landslides may occur may be based on an analysis of those factors and their relationship to the area's previous landslides. Landslides are spatially distributed and have a high density depending on the topography, weather, geology, land use and anthropogenic causes (Khan et al., 2019). In order to understand how the landslides, occur and subsequently create a map of landslide susceptibility, it is crucial to evaluate the impact of these causal factors based on the spatial distribution of landslides. In the present study, slope, aspect, curvature, distance to lineament, distance to stream, land use/land cover, lithology and rainfall have been considered as causative elements used to prepare landslide susceptibility mapping. The following will provide a detailed explanation of how each causative factor influences the landslide occurrence.

Slope

The investigation of landslides is significantly influenced by slope angle, directly association with landslide susceptibility mapping (Yalcin and Bulut, 2007). As slope angles increase, the probability of landslide occurrence increases as the slope angle decreases due to gravity, resulting in a lower frequency of landslide events on gentler slopes compared to steeper ones (Kumar et al., 2015). Steeper slopes are typically characterized by a greater susceptibility to sliding (Hamza and Raghuvanshi, 2016). In this study, slopes were classified into five categories (0-7^0, 7^0-14^0, 14^0-23^0, 23^0-36^0, and >36^0) based on the natural breaks' method, as it clearly classifies the slope with the existing topography of the study area in comparison with other classification methods.

The result showed that lower slope angles have a lower frequency of landslides, but their frequency increases as the slope angle increases. In most studies of landslides, slope steepness is considered as the major causative factor of landslide occurrence (Asmelash and Barbieri, 2012). If the slope is steeper, it is more susceptible to instability as compared to gentle slopes (Ayele, 2014). Gentle slopes are expected to have a low frequency of landslides because they possess lower shear stresses associated with low gradients (Raghuvanshi et al., 2015).

Erden and Karaman (2012) suggested that this parameter has been considered one of the most important factors in landslide susceptibility modeling.

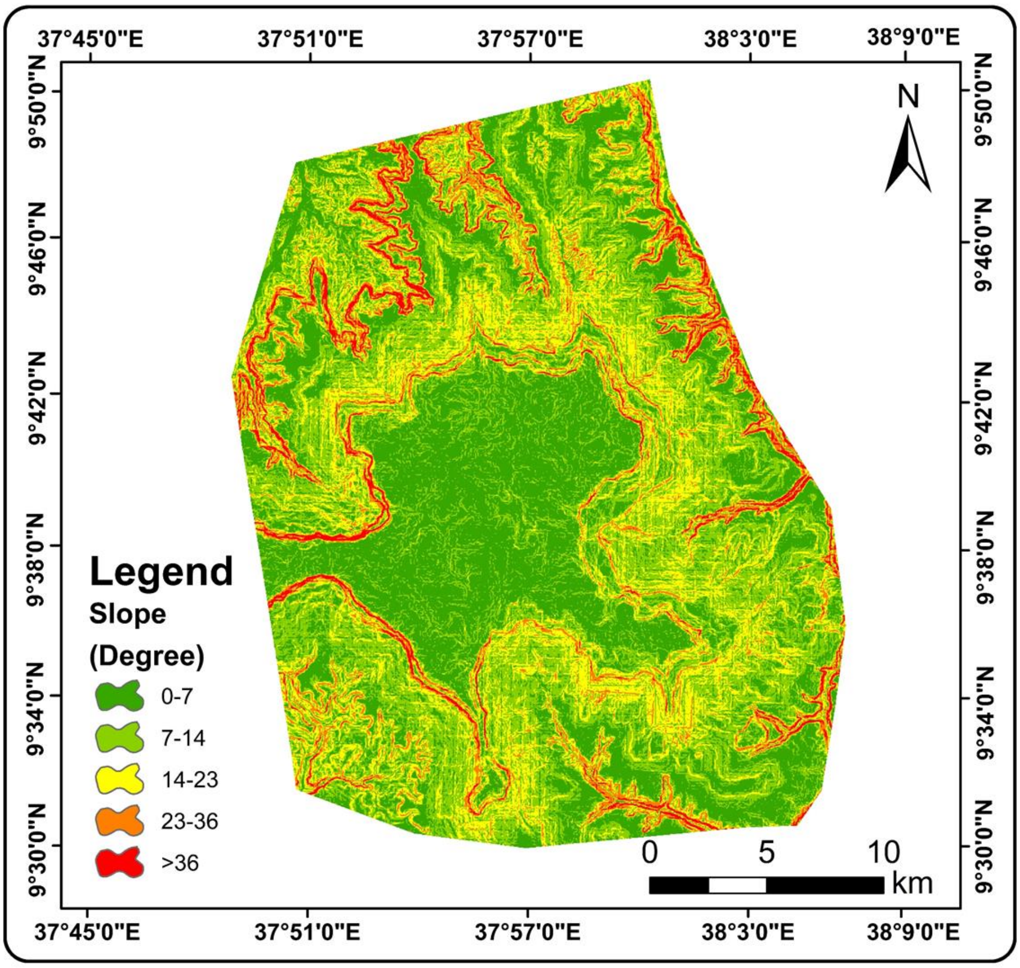

Figure 5 Slope map

Aspect

As stated by Xu et al. (2012), aspect is the direction in which the maximum slope of the terrain is oriented. It is often quantified in terms of degrees from 0 to 360, signifying slope orientation (Mersha and Meten 2020). The slope aspect might affect the beginning of a landslide as it affects moisture retention and vegetation cover (Raghuvanshi et al. 2015). The aspect of the study area is classified into N, NE, NW, S, SE, SW, E, W and flat.

The aspect factor map was derived from the DEM of the study area with a spatial resolution of 30m. The aspect map was grouped into nine classes Flat (-1°), North (0°-22.5°; 337.5°-360°), Northeast (22.5°-67.5°), East (67.5°-112.5°), Southeast (112.5°-157.5°), South (157.5°-202.5°), Southwest (202.5°-247.5°), West (247.5°-292.5°) and Northwest (292.5°-337.5°) as shown in Figure 6a.

The results indicate that 16.34% of the landslide occurred in the north-facing slopes, 15.77% occurred in the northeast-facing slopes while 14.59% in the northwest-facing, 13.81% in the west facing and 12.03% in the southwest facing slopes. This shows that slopes facing the north, northeast, northwest, west, and Southwest have a high correlation with landslides. This result agrees with a study conducted by Chimidi et al. (2017) in which slopes oriented towards southwest, west, and northwest showed a high probability of landslide occurrence. The landslides which occurred in the east (67.5°-112.5°), south (157.5°-202.5°) and southeast (112.5°-157.5°) facing slopes have less impact on slope failure of the area (Table 3).

Curvature

The curvature of the study area was derived from a digital elevation model (DEM) with a spatial resolution of 30 meters, and it was categorized into three classes. Large negative values represent concave curvature, values near zero indicate a flat terrain, and large positive values signify convex curvature. Concave curvature is associated with a higher probability of groundwater occurrence and this groundwater has its own influence on slope instability. Conversely, when the slope curvature is convex, it creates favorable conditions for slope erosion. According to Riaz et al. (2018) and Wubalem (2021), curvature influences slope instability due to erosion and groundwater accumulation.

Among the total area, flat curvature is the most dominant one, which covers a large area as compared to the concave and convex ones, respectively (Figure 6b). As a result, concave and convex aspect classes are highly influencing the landslide occurrence as compared to the flat curvature. Accordingly, the maximum values were assigned for the curvature classes within negative and positive values. These curvature classes are zones of groundwater accumulation and divergence, respectively. The negative values are zones of groundwater percolation into the soil/rock mass. Further, a flat area was assigned with the lowest susceptibility to landslide, which is in agreement with Girma (2015), Chen et al. (2016), and Ayele (2019) in which landslide activity increases with negative and positive values of curvature. According to the topographic type, the value is higher in the hilly and mountainous areas and low in flat areas (Lee and Min, 2002).

Lithology

Lithology serves as one of the contributing factors to landslides (Riaz et al., 2018; Berhane et al., 2020). Landslide susceptibility tends to rise when the underlying rock unit is loose and fractured. In this study, a lithological map of the study area was prepared from existing 1:250,000 geological maps of the Addis Ababa sheet provided by GSE.

The results of lithology from the existing map showed that the study area contains seven lithological units, namely Quaternary Superficial sediment (QSS), Residual soil, alluvial deposits, Basalt, Limestone, Gohatsion Formation, and Sandstone (Figure 6c). The result showed that Sandstone and alluvial soil cover the highest and lowest area coverage in percent, respectively as shown in Table 2.

Land use/land cover

Land use/land cover changes globally significantly influence on rainfall-triggered landslides (Mersha and Meten, 2020). Activities like deforestation, overgrazing, and steep-slope cultivation, driven by human intervention, lead to land use and cover alterations, often initiating slope instability (Glade, 2003). Vegetation plays a crucial role in withstanding slope movement as well as stability through its extensive root network, enhancing lithological shear resistance. Conversely, sparsely vegetated or barren slopes are prone to erosion, thereby intensifying slope instability (Sharma et al., 2012). The land use map of the study area was, generated from the 2023 Google Earth image and analyzed in ArcGIS, it identifies seven land-use types: dense forest, sparse forest, shrub, grassland, agricultural land, settlement, and water bodies, with an agricultural land predominating in the area (Figure 6b).

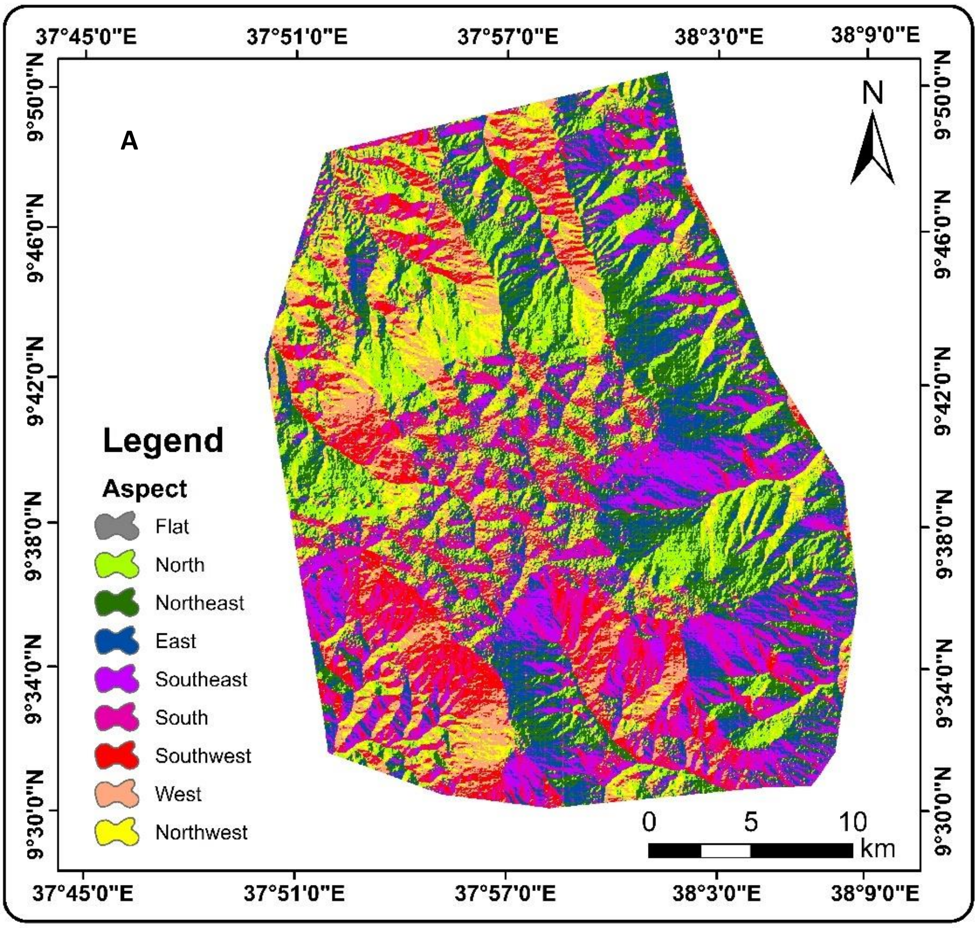
37°45'0"E
37°51'0"E
37°57'0"E
38°3'0"E
38°9'0"E
9°50'0"N
9°46'0"N
9°42'0"N
9°38'0"N
9°34'0"N
9°30'0"N
A
N
Legend
Aspect
Flat
North
Northeast
East
Southeast
South
Southwest
West
Northwest
0 5 10
km

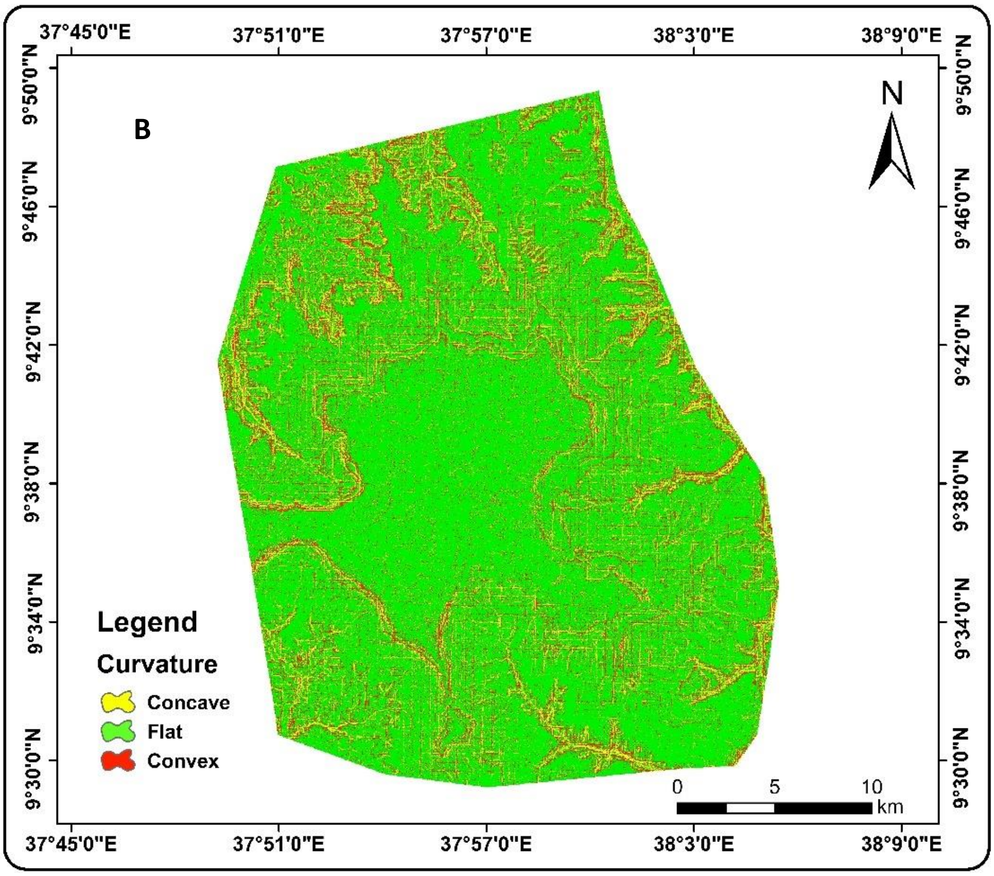
37°45'0"E
37°51'0"E
37°57'0"E
38°3'0"E
38°9'0"E
9°50'0"N
9°46'0"N
9°42'0"N
9°38'0"N
9°34'0"N
9°30'0"N
B
N
Legend
Curvature
Concave
Flat
Convex
0 5 10
km

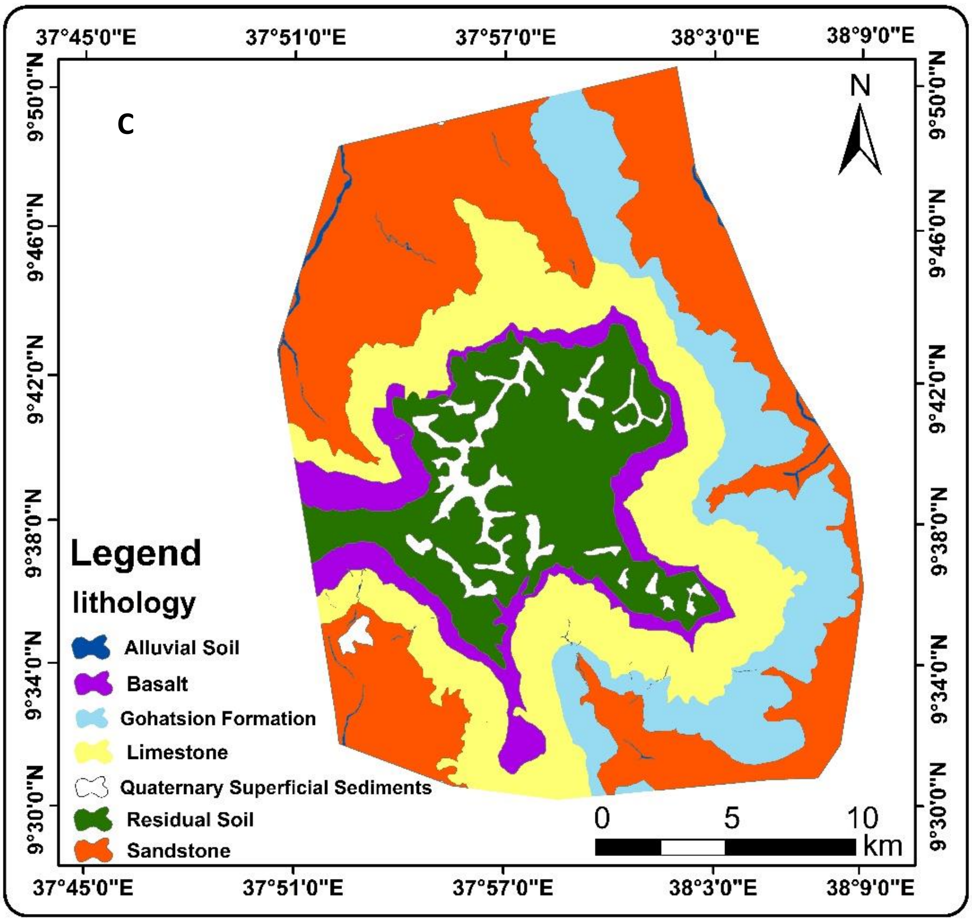

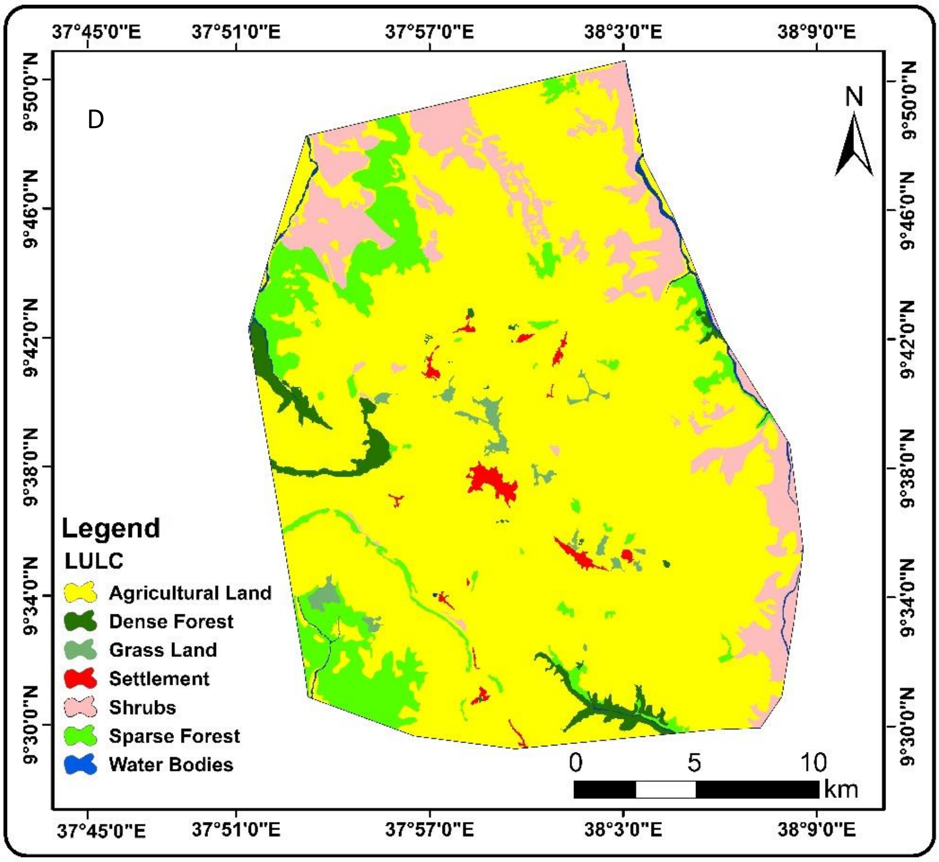

Figure 6 a) Aspect, b) Curvature, c) lithology, d) Land use/land cover

Distance to Lineament

Lineaments affect surface material structures and significantly influence the topography permeability and, thus, slope stability. The proximity of a slope to these features influences its stability, increasing the susceptibility of a slope to landslide occurrence (Samanta 2016). Lineament data were extracted from Google Earth images. The lineament factor was characterized as proximity analysis by the use of the Euclidian distance buffering tool, and the distance to lineament factor was reclassified based on manual classification methods into eight classes: 0-200m, 200-400m, 400-600m, 600-800m, 800m-1000m, 1000m-1200m, 1200m-1400m, and >1400m. The classification was made with manual classification to be realistic on the relationship of landslides with lineament or escarpment.

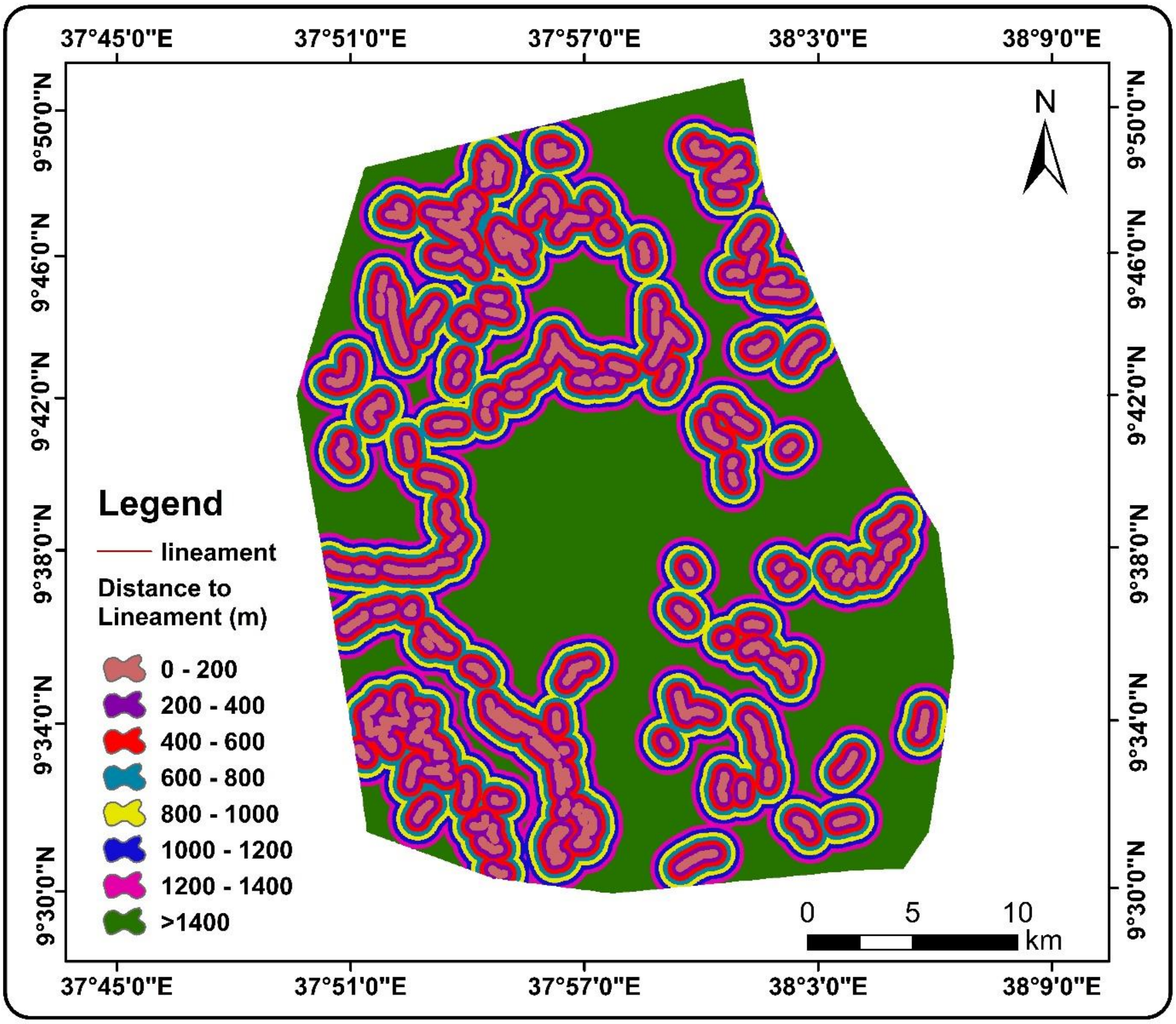

Figure 7 Distance to lineament map

Distance to Stream

Streams play a crucial role in landslide susceptibility, especially when they undercut slope bases. This parameter is essential for controlling various types of landslides in the area (Che et al. 2011). Numerous unnamed streams and named- streams like Busiyo, Oranisa, Fino, and Urgaha streams run through the study area. These streams are also the source of many landslides that frequently undercut slopes near them. So, in the landslide susceptibility study, this parameter was considered an important factor. The most probable landside locations are in zones with parallel drainage patterns on steep slopes. In the current study, streams were digitized from a 1:50,000 scale topographic map and then the distance to stream map was generated using Euclidean distance buffering analysis in ArcGIS and reclassified by manual methods of classification to be realistic on the relationship of landslides with stream.

The stream map of the area was classified into eight classes: 0 – 100m, 100m – 200m, 200m – 300m, 300m – 400m, 400m -500m, 500m - 600m, 600m – 700m and greater than 700m. The classification was made with a manual classification method to describe its realistic relationship with landslides.

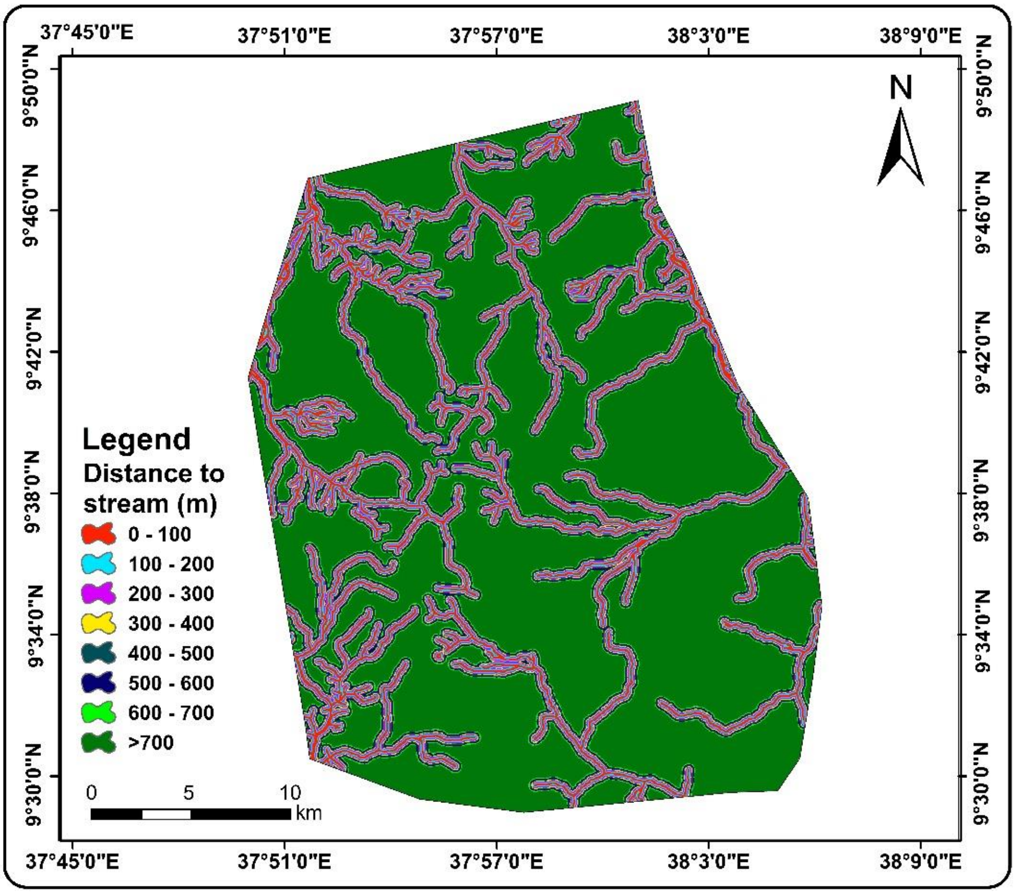

Figure 8 Distance to stream map

Rain fall

High annual rainfall, in five rainy seasons, saturates the soil and creates positive pore pressure, contributing to landslide susceptibility (Broothaerts et al., 2012). Annual rainfall data, and spatial distribution, were sourced from the National Meteorological Agency of Ethiopia. Interpolation using the Inverse Distance Weighted (IDW) method in ArcGIS was employed to estimate rainfall at Fincha, Kachise, Shukute, Jeldu, Abay skeleko, and Yejube stations, relying on the assumption that an unknown point's value is a weighted average of known values in its neighborhood. IDW is favored for its intuitive and efficient nature (Azpurua and dos Ramos, 2010). The Rainfall factor map, extracted from the interpolated data of six rain gauge stations using the extract by mask tool in ArcGIS, was classified into five ranges through natural break classification to accommodate uneven data distributions. The rainfall data analysis showed that the maximum monthly rainfall occurs in June, July, August, and September, coinciding with the landslide occurrence in this area. The rainfall map of the study area was divided into five annual rainfall classes of 1455 – 1566, 1566 – 1613, 1613 – 1666, 1666 – 1724, and 1724 - 1794 millimeters (Figure 9) which was reclassified by the natural break's method.

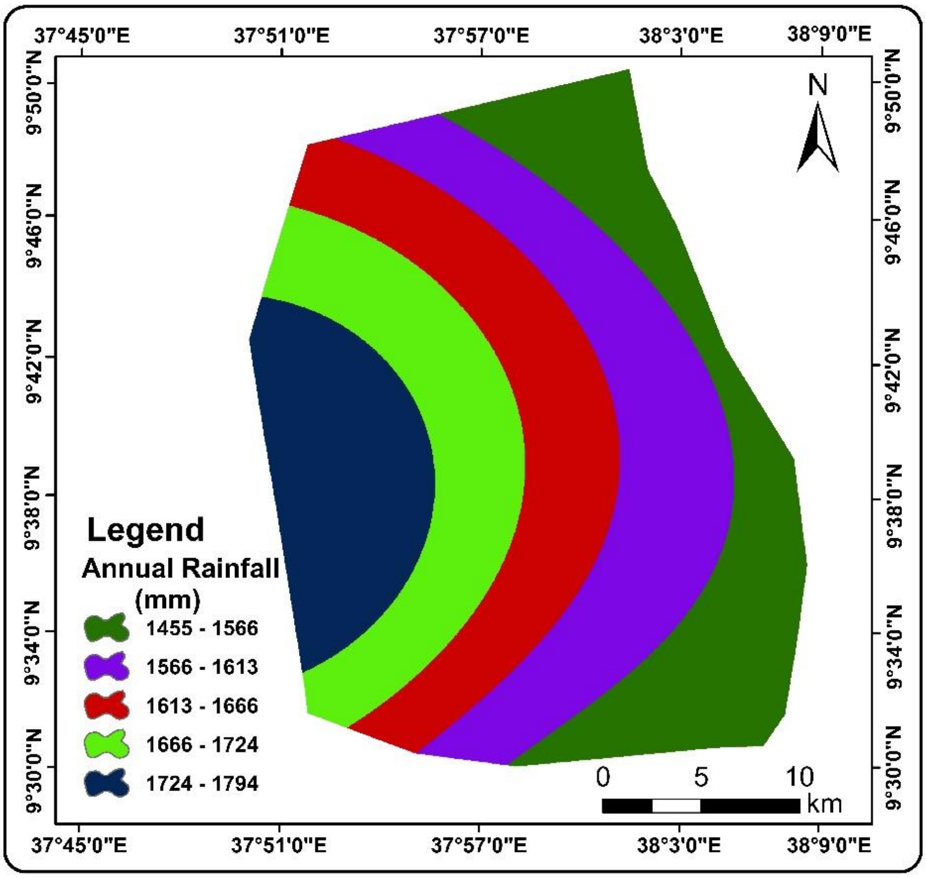

Figure 9 Average annual rain fall map

5.3 Relationship between landslide and causative factors

Using the statistical frequency ratio and regression models, this study examined the relationships between eight potential causes of landslides. The causal factors were classified into fifty-three classes (Table 3), which assigns the weights assigned to each class of the FR model. The weight values obtained from the FR model illustrate the spatial relationship of the causative factor classes to landslide occurrence. In this study, the relationship between landslides and each class of causative factors (slope, aspect, curvature, distance to stream, distance to lineaments, rainfall, lithology, and land use/land cover) was examined and shown in the following figure (Figure 10).

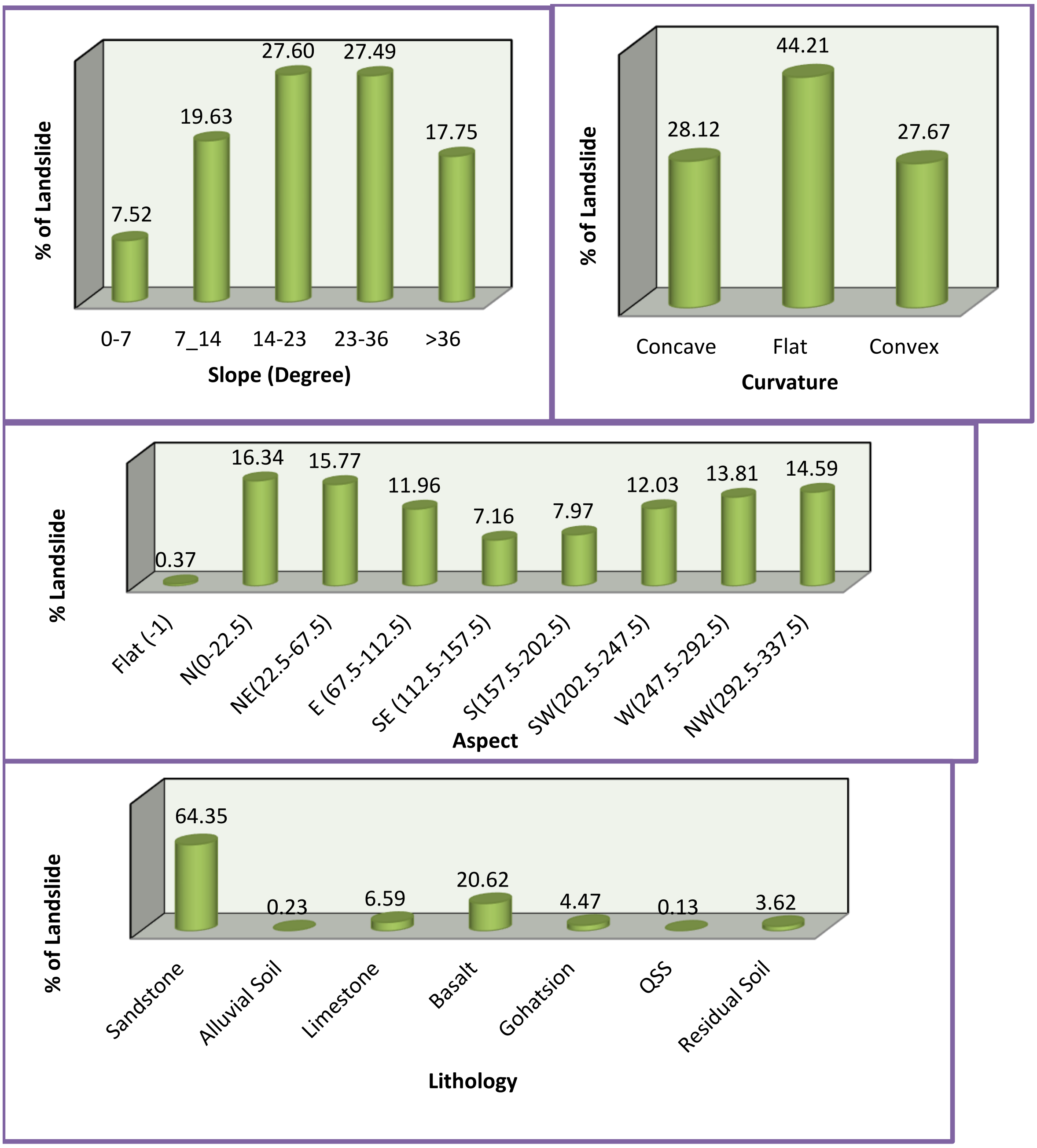

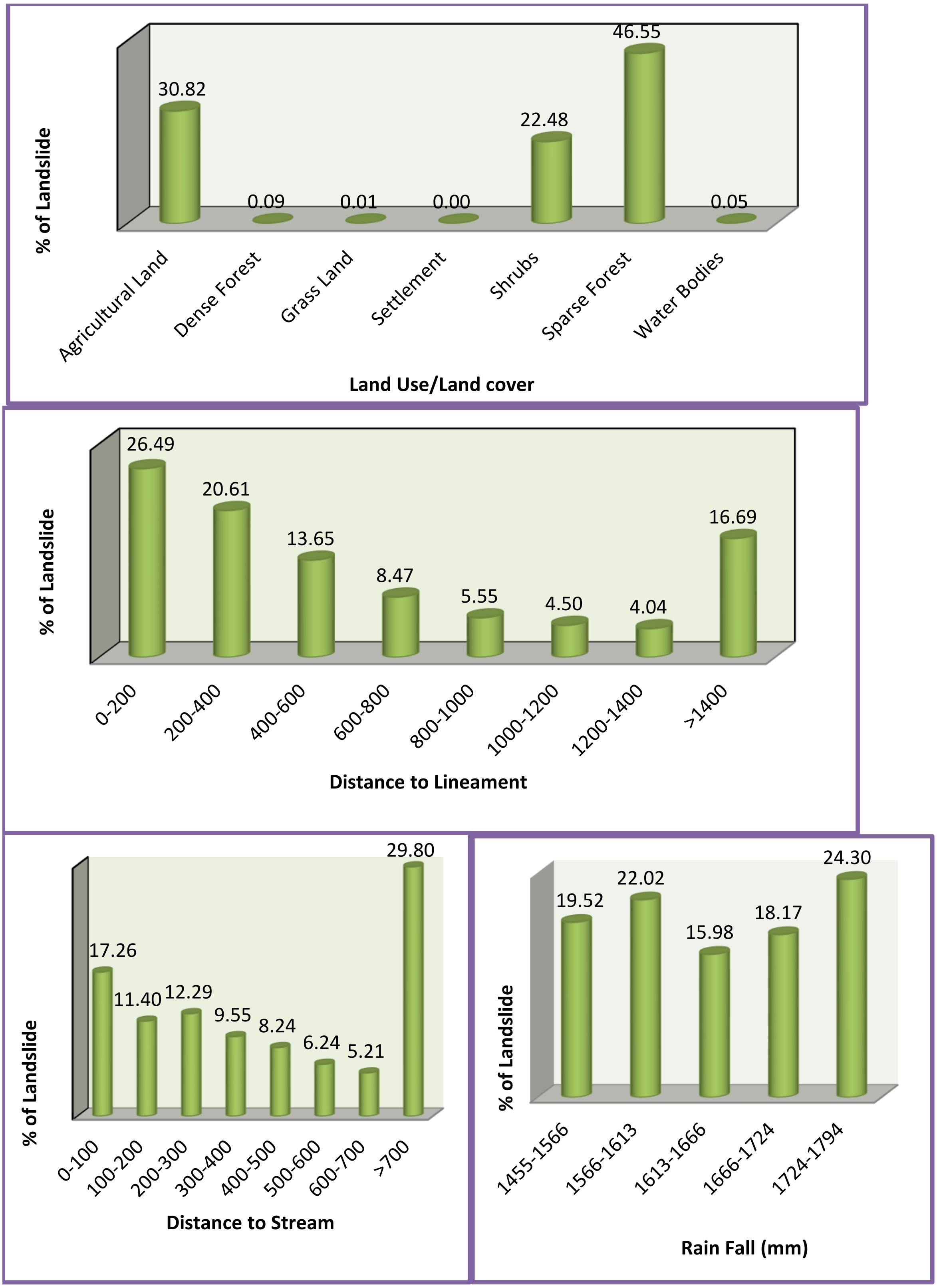

Figure 10 Relationship of landslide occurrence with the causative factors

5.4 Rating Landslide Factors using Frequency Ratio and Logistic Regression Model

5.4.1 Frequency Ratio Model

The FR values increase with increasing slope angle. For example, the slope classes of 14-23^0, 23-36^0 and above 36^0 have the highest FR values of 1.233, 3.054, and 4.853, respectively. However, the classes with lower slope angles have the least FR values with the least probability of landslide occurrence. The results is in agreement with the finding of Mersha and Meten (2020) found that slope classes > 12^0 have a higher contribution to landslide occurrence (This correlation indicated that the landslide probability increases as the slope gradient increases. The aspect analyses showed that the maximum FR value (1.457) was for the Northwest, followed by West (1.278), North (1.257), Northeast (1.015), and Southwest (1.119), indicating a higher probability of landslide occurrence. The other aspect classes have less than zero FR values, which indicate a lower probability of landslide occurrence. The results in this study area in agreement with Getachew and Meten (2021), in which the north, southwest, west, and northwest face a high probability of landslide occurrence. This is also in line with Addis (2022), which reported that the southwest, west, and northwest-facing slopes had a high probability of landslide occurrence.

In the case of curvature, the FR is higher for a convex slope (1.726), and for a concave slope, the FR value is 1.765. The other curvature (flat) indicates lower values (0.650). This agrees with (Mersha and Meten 2020) reported that concave and convex slopes are highly probable for landslide occurrence, because of the effects of slope shape for rainwater impounding and gravity effect.The FR for distance to stream clearly showed that the class of 0 - 100m, 100 - 200m, 200 – 300m, 300 – 400m, and 400 – 500m have the highest influence on landslide occurrence with values of 1.390, 1.138, 1.238, 1.210, and 1.073 respectively. The remaining classes of 500–600 m, 600–700 m, and above 700m have a lower probability of landslide occurrence with FR values of 0.949, 0.924, and 0.748, respectively. For distance to lineaments, the intervals 0 – 200m, 200 – 400m and 400 – 600m have a higher probability of landslide occurrence with values of 3.403, 2.130, and 1.330, respectively. For the lithology factor, frequency analysis shows that the basalt and sandstone have the highest susceptibility to landslides with FR values of 2.781 and 1.913, respectively. For rainfall, the class of 1724 - 1794 mm/year has the highest influence on landslide occurrence with a value of 1.464. The other rainfall classes indicated the lower FR values. For land use and land cover, shrub and sparse forest have higher FR values of 2.160 and 4.410 respectively.

Table 3 Rating of each factor class from a spatial relationship between each factor class and landslide using frequency ratio model

Factor	Class	NCP	% NCP	NLP	% NLP	SR (a)	CR (b)	FR = a/b
Slope	0-7	280372	28.017	5461	7.524	0.075	0.280	0.296
	7 to 14	369626	36.936	14246	19.629	0.196	0.369	0.531
	14-23	224031	22.387	20032	27.601	0.275	0.224	1.233
	23-36	90077	9.001	19954	27.494	0.275	0.090	3.054
	>36	36603	3.658	12884	17.752	0.178	0.037	4.853
Total		1000709		72577				
Aspect	Flat (-1)	7105	0.710	266	0.367	0.004	0.007	0.516
	N (0-22.5),(337.5 – 360)	130072	12.998	11858	16.339	0.163	0.130	1.257
	NE (22.5-67.5)	155522	15.541	11447	15.772	0.158	0.155	1.015
	E (67.5-112.5)	161650	16.154	8680	11.960	0.120	0.162	0.740
	SE (112.5-157.5)	123498	12.341	5196	7.159	0.072	0.123	0.580
	S (157.5-202.5)	106931	10.686	5787	7.974	0.080	0.107	0.746
	SW (202.5-247.5)	107614	10.754	8733	12.033	0.120	0.108	1.119
	W(247.5-292.5)	108160	10.808	10024	13.812	0.138	0.108	1.278
	NW (292.5-337.5)	100157	10.009	10586	14.586	0.146	0.100	1.457
Total		1000709		72577				
Curvature	Concave	159409	15.930	20411	28.123	0.281	0.159	1.765
	Flat	680864	68.038	32087	44.211	0.442	0.680	0.650
	Convex	160436	16.032	20079	27.666	0.277	0.160	1.726
Total		1000709		72577				
Lithology	Sandstone	336559	33.632	46701	64.347	0.643	0.336	1.913
	Alluvial Soil	5470	0.547	166	0.229	0.002	0.005	0.418
	Limestone	233117	23.295	4781	6.587	0.066	0.233	0.283
	Basalt	74206	7.415	14965	20.619	0.206	0.074	2.781
	Gohatsion Formation	154398	15.429	3245	4.471	0.045	0.154	0.290
	Quaternary superficial sediment	31139	3.112	92	0.127	0.001	0.031	0.041
	Residual Soil	165820	16.570	2627	3.620	0.036	0.166	0.218
Total		1000709		72577				

Land use/land cover	Agricultural Land	766369	76.584	22370	30.822	0.308	0.766	0.402
	Dense Forest	923	0.092	67	0.092	0.001	0.001	0.000
	Grass Land	9327	0.932	4	0.006	0.000	0.009	0.000
	Settlement	7901	0.790	0	0.000	0.000	0.008	0.000
	Shrubs	104130	10.406	16315	22.480	0.225	0.104	2.160
	Sparse Forest	105609	10.554	33782	46.546	0.465	0.106	4.410
	Water Bodies	6435	0.643	39	0.054	0.001	0.006	0.000
Total		1000709		72577				
Distance to Lineament	0-200	77904	7.785	19229	26.495	0.265	0.078	3.403
	200-400	96867	9.680	14961	20.614	0.206	0.097	2.130
	400-600	102689	10.262	9905	13.648	0.136	0.103	1.330
	600-800	99099	9.903	6144	8.465	0.085	0.099	0.855
	800-1000	96278	9.621	4029	5.551	0.056	0.096	0.577
	1000-1200	87244	8.718	3264	4.497	0.045	0.087	0.516
	1200-1400	77649	7.759	2931	4.038	0.040	0.078	0.520
	1400-1600	362979	36.272	12114	16.691	0.167	0.363	0.460
Total		1000709		72577				
Distance to Stream	0-100	124288	12.420	12530	17.264	0.173	0.124	1.390
	100-200	100276	10.020	8274	11.400	0.114	0.100	1.138
	200-300	99404	9.933	8922	12.293	0.123	0.099	1.238
	300-400	78979	7.892	6930	9.548	0.095	0.079	1.210
	400-500	76892	7.684	5981	8.241	0.082	0.077	1.073
	500-600	65830	6.578	4532	6.244	0.062	0.066	0.949
	600-700	56374	5.633	3779	5.207	0.052	0.056	0.924
	>700	398666	39.838	21629	29.801	0.298	0.398	0.748
Total		1000709		72577				
Rain Fall	1455-1566	208640	20.849	14170	19.524	0.195	0.208	0.936
	1566-1613	238093	23.792	15985	22.025	0.220	0.238	0.926

	1613-1666	200181	20.004	11598	15.980	0.160	0.200	0.799
	1666-1724	187719	18.759	13186	18.168	0.182	0.188	0.969
	1724-1794	166076	16.596	17638	24.302	0.243	0.166	1.464
Total		1000709		72577				

Where NCP is a number of class pixels, %NCP is the percentage of no class pixels, NLP is a number of landslide pixels, %NLP is the percentage of no of landslide pixels, SR is a slide ratio, CR is a class ratio, and FR is the frequency ratio.

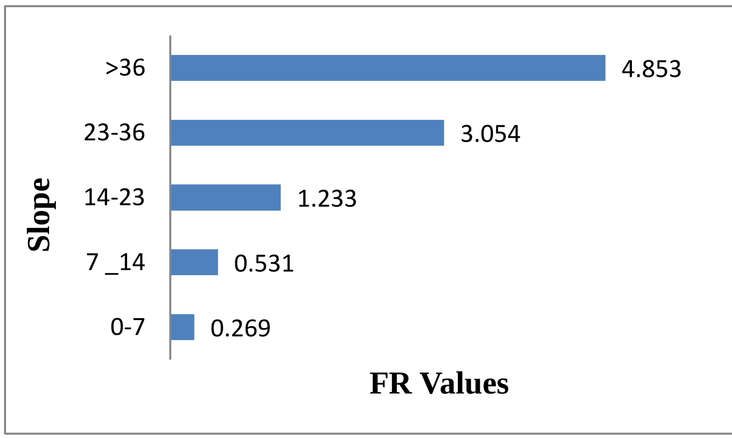

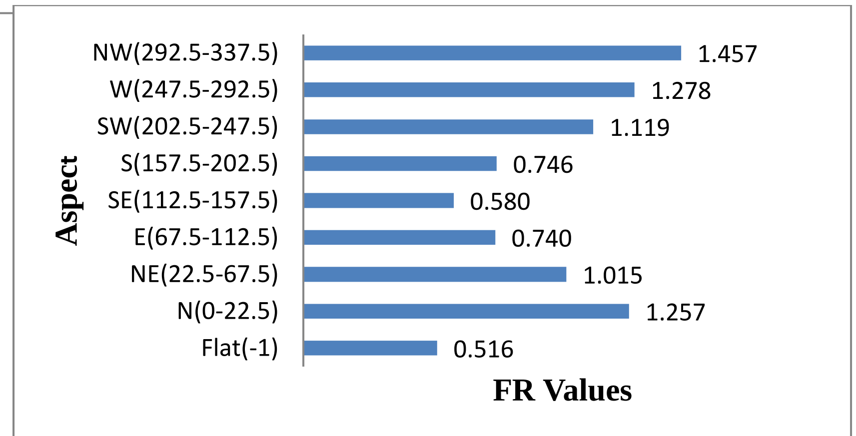

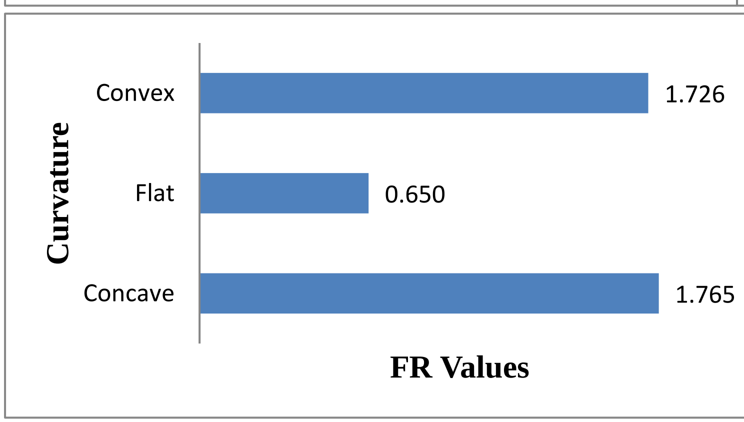

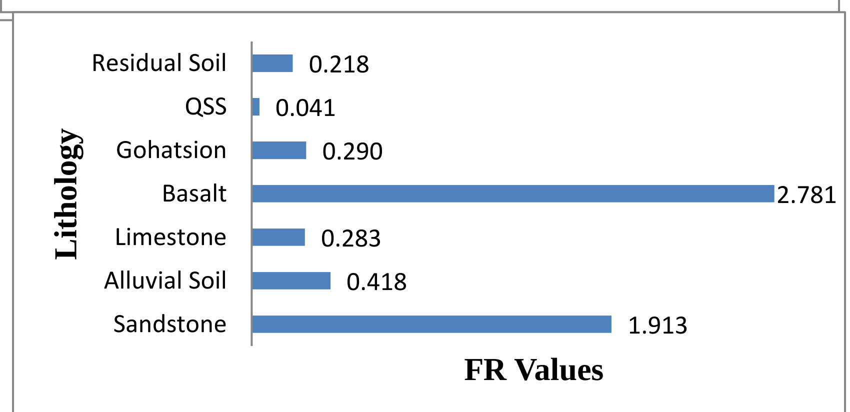

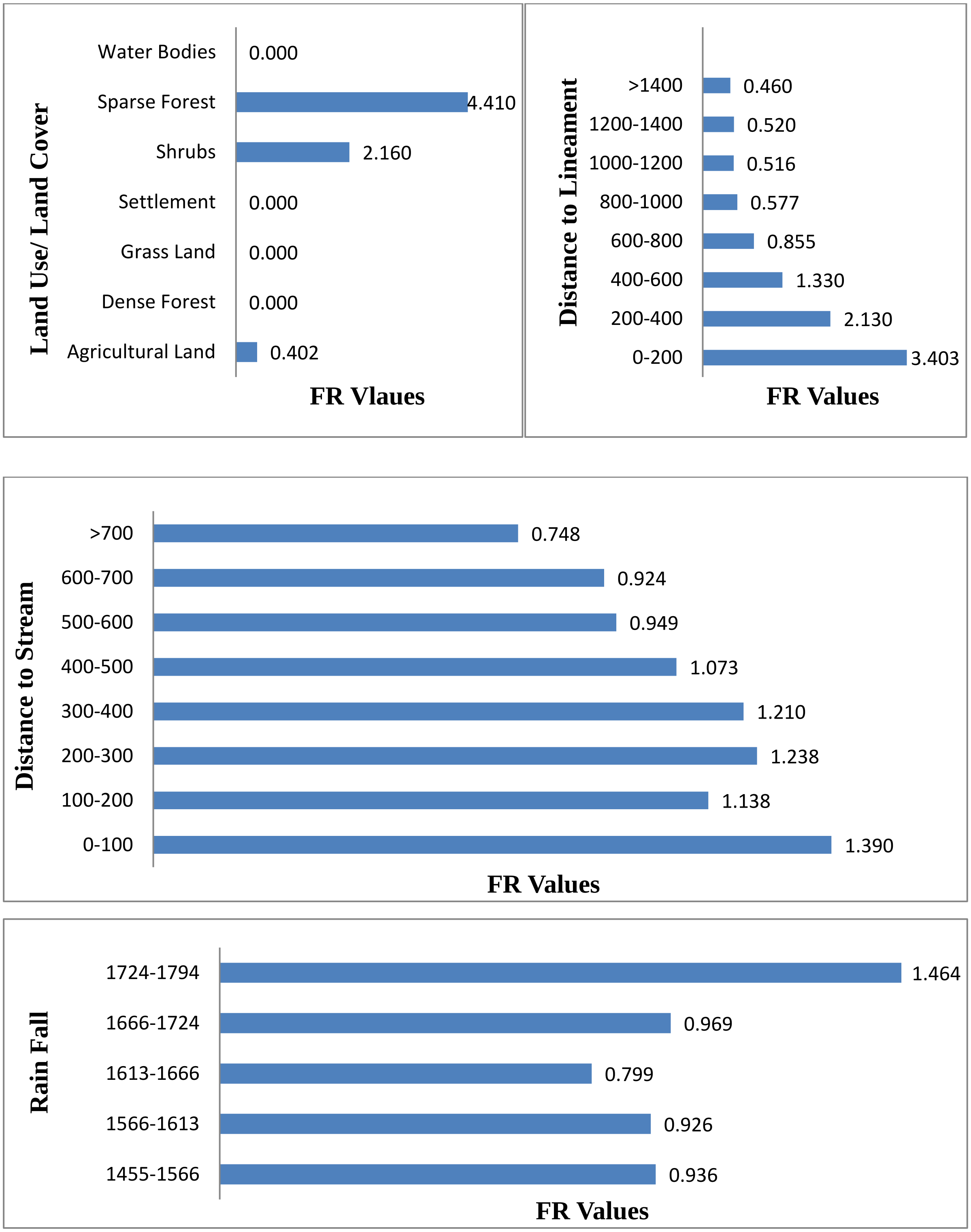

Figure 11 Relationship between causative factors and frequency ratio values

5.4.2 Logistic Regression Model

Logistic regression analysis has been performed using the standard statistical software package of SPSS. For the purposes of data sampling in the logistic regression model, there are three methods that can be used. The first is to use data from all over the study area, which results in unequal proportions of landslide and non-landslide pixels (Guzzetti et al., 1999; Ohlmacher and Davis, 2003); the second is to use all the landslide pixels and equal proportions of non-landslide pixels, which may reduce the amount of data to be used but eliminates the associated bias in the data sampling. The third most reasonable method is partitioning the landslide pixels into training and validation datasets. The logistic regression model uses an unequal combination of pixels from landslides and non-landslides points in this study. The model outputs from logistic regression analysis in SPSS software were obtained by inputting the conditional variables, as shown in Appendix II. The resulting the Coefficients of Logistic regression method for Independent variables are shown in Table 4.

Z = -5.671 + 0.104*Stream + 0.189*Aspect + 0.331*Curvature + 0.472*Lineament + 0.559*Lithology + 0.410*LULC + (0.370) *Rainfall + 0.450*Slope as equation (5)

Where, Z is the linear combination

Table 4 Logistic Regression (LR) coefficients, collinearity test and model statistics

Factors	**LR coefficient**	**Collinearity Statistics**			
		Tolerance	VIF	Modal statistics	Values
(Constant)	-5.671	.937	1.137	Cox & Snell R Square	0.309
Stream	.104	.967	1.305	Nagelkerke R Square	0.531
Aspect	.189	.994	1.219	Chi-square	26.13
Curvature	.331	.875	1.056	Significance	0.01
Lineament	.472	.852	1.173		
Lithology	.559	1.000	1.000		
LULC	.410	.965	1.137		
RF	.370	.814	1.138		
slope	.450	.946	1.147		

VIF, variance inflation factor

Factors with positive values of logistic regression coefficient showed a positive correlation towards landslide occurrence, while that independent variable with negative coefficients showed a negative correlation (Yalcin et al., 2011; Prakash, 2015; Meten et al., 2015). As shown in Table 4 above, all independent variables positively correlate with landslide occurrences based on the LR coefficient in this study.

Multicollinearity and Hosmer-Leme show tests were considered in logistic regression analysis to obtain the best results (Prakash, 2015; Wubalem and Meten, 2020). For multicollinearity diagnosis, tolerance (TOL) and variance inflation factor (VIF) are the two crucial indices. A serious multicollinearity between independent variables occurs when the tolerance values are smaller than 0.1 and a VIF value is greater than 10 (Paper, 2013). The tolerance and VIF values in this study are estimated and shown in Table 4, indicating that there is no multicollinearity between any of the variables considered in this study.

5.5 Landslide Susceptibility Mapping

In this study, the landslide susceptibility maps were quantitatively prepared using the bivariate and multivariate statistical analysis techniques particularly frequency ratio and logistic regression models, respectively in a GIS environment. Weight of each causative factor class was defined by the combination of each parameter and landslide inventory map. By combination of following decision rules (addition, division, multiplication, and subtraction), the weight of each conditioning factor class was defined. Finally, the landslide susceptibility index classification using the natural breaks method was done as it is well suited to evenly distributed data.

5.5.1 Landslide Susceptibility Mapping Using Frequency Ratio Model

From the raster calculation, the final result of LSI values of the study area ranges from 3.489 to 21.523. The LSI map was classified into five classes using the natural breaks method this method is used because it is best for uneven data distribution, and it is capable of classifying the landslide susceptibility index map into a different category based on the inherent data value similarity (Meten et al., 2015). Therefore, the LSI values were classified into five susceptibility areas: very low (3.489 – 4.851), low (4.851 – 5.800), moderate (5.800 – 7.211), high (7.211 – 12.281) and very high (12.281 – 21.523) [Figure 13].

Table 5 FR Landslide susceptibility class based on landslide susceptibility index

Susceptibility classes	LSI	Pixels	Area (km^2)	Area (%)
Very Low	3.489 – 4.851	90608	81.55	9
Low	4.851 – 5.800	209376	188.44	21
Moderate	5.800 – 7.211	237882	214.09	24
High	7.211 – 12.281	341640	307.48	34
Very High	12.281 - 21.523	121185	109.07	12

The landslide susceptibility map (Figure 12 and Table 5) clearly shows that in the study area, 81.55km^2 (9%) falls in very low susceptible classes and 307.48 km^2 (34%) of the area falls in high susceptibility classes while the remaining ones including 188.44km^2 (21%), 214.09km^2 (24%), and 109.07km^2 (12%) of the study area fall in low, moderate and very high susceptibility classes respectively, were estimated from the ratio of the product of pixels and 30m*30m cell size to 10^6. Where 10^6 is the unit conversion from meter to kilometer.

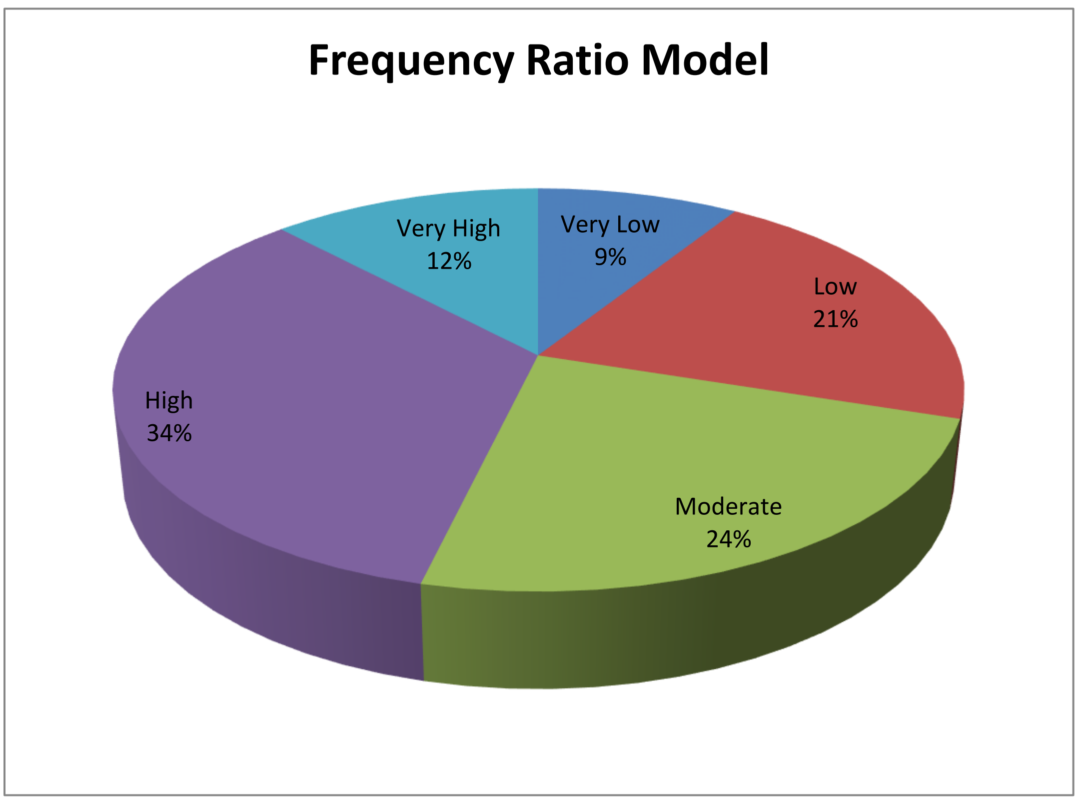

Figure 12 Distribution of landslide susceptibility classes frequency ratio in the study area

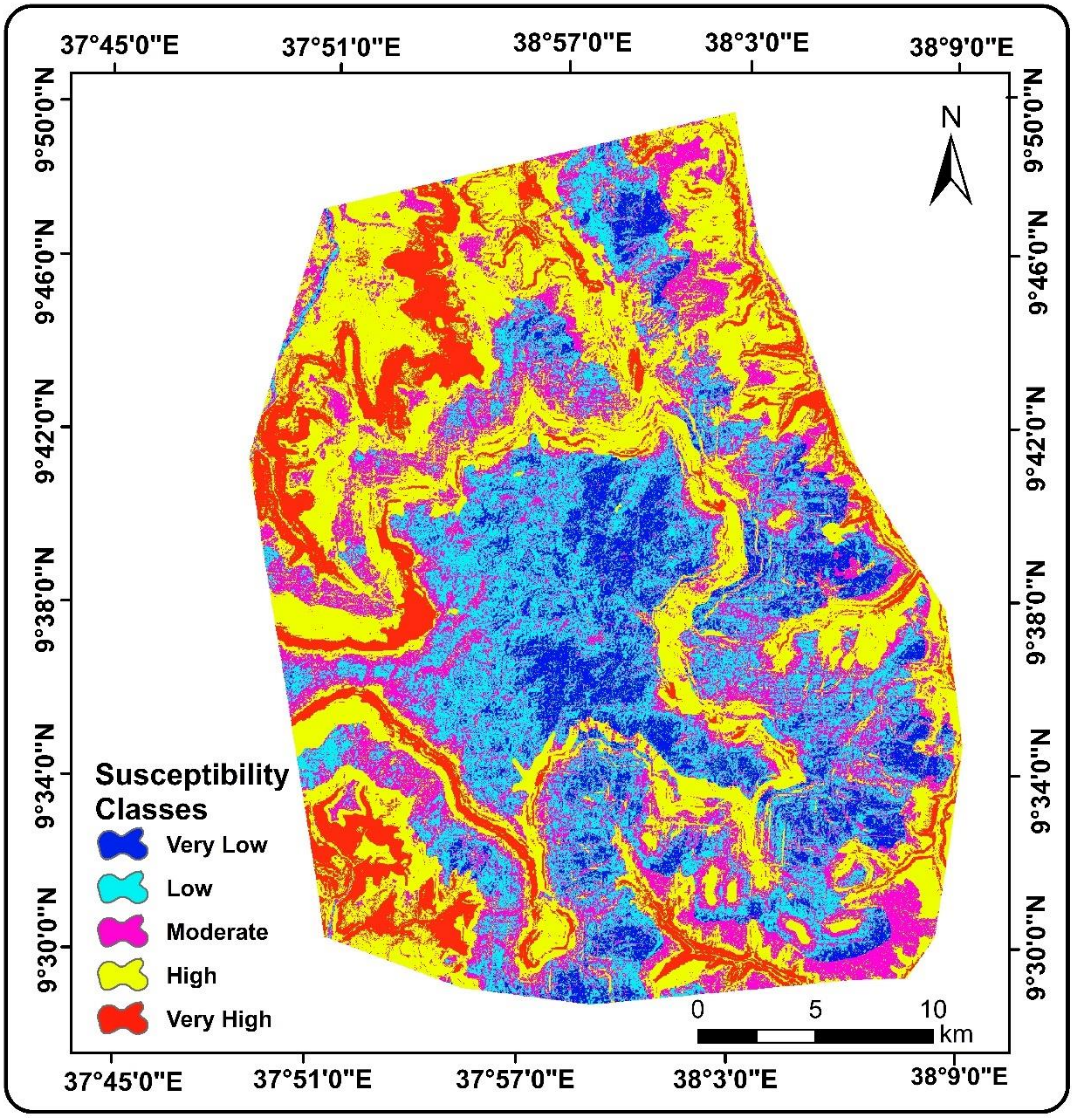

Figure 13 Landslide Susceptibility map using frequency ratio

5.5.2 Landslide Susceptibility Mapping Using Logistic Regression Model

From the 3D analyst tools of raster math and spatial analyst tools of raster calculator, the final result of probability values of the study area ranges from (0.0760 to 0.9481) as shown in Table 6. The LSI map was classified into five classes using the natural breaks method this method is used because it is important for uneven data distribution and is capable of classifying the landslide susceptibility index map into different categories based on the inherent data value similarity (Meten et al., 2015).

Table 6 LR Landslide susceptibility class based on landslide susceptibility index

Susceptibility classes	**LSI**	**Pixels**	**Area (km^2)**	**Area (%)**
Very Low	0.0760 – 0.0792	72486	65.24	7
Low	0.0792 – 0.0849	325323	292.79	33
Moderate	0.0849 – 0.090	87681	78.91	9
High	0.090 - 0.0708	284230	255.81	28
Very High	0.1375 – 0.9481	230971	207.87	23

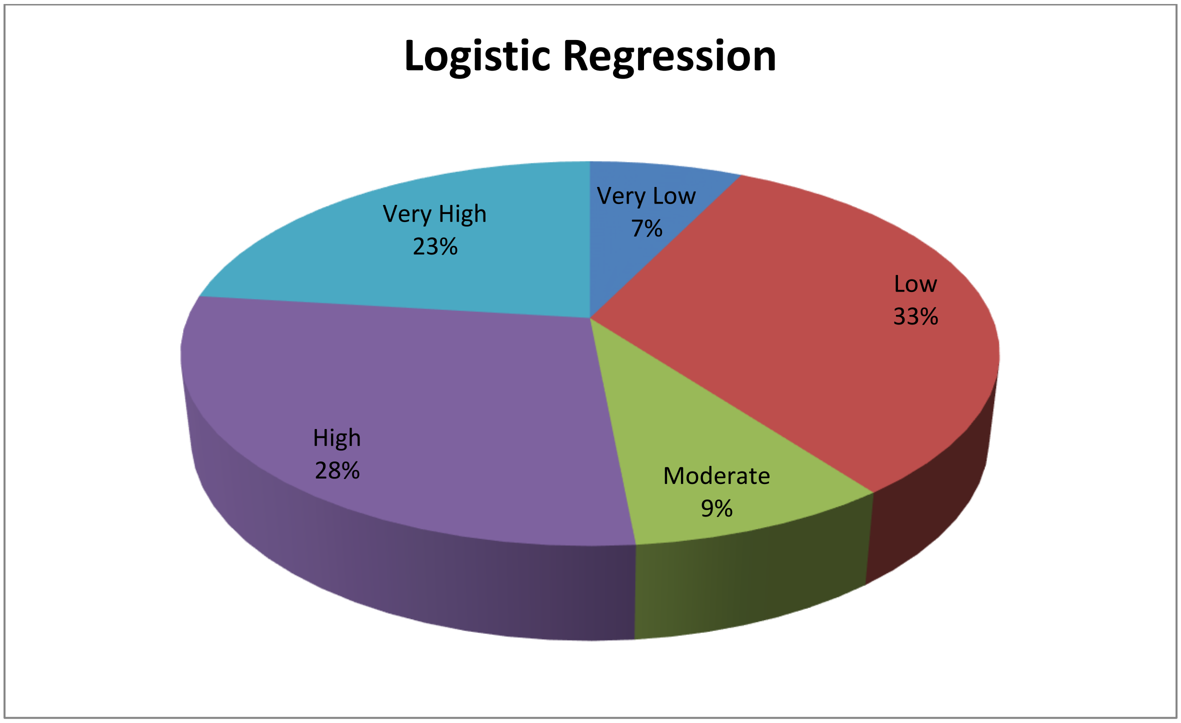

Figure 14 Distribution of landslide susceptibility classes logistic regression in the study area

As shown in Figures 13 and 15, the plateau part of the study area, including the localities of Serbadi, Mudema, Guduru, Obora, Gerbi Gole, Danisa, Mudi Ula Kera, Insilale, Debeka, most parts of Goro Jalate and Mukarba showed very high and high susceptibility classes. Localities of Sotelo, Dokonu Sure, Arbi Gebiya, Deso, Gute Andode, Goho Guduru, Gago, Gugsa Goro, Irjajo, Haro, Mandida Tunjiti, and Gute Sembo fall in very low, low and moderate susceptibility classes. In general, most of the western and eastern part of the study area falls under high and very high susceptibility zones. Very low, low, and moderate susceptibility classes are distributed throughout the study area.

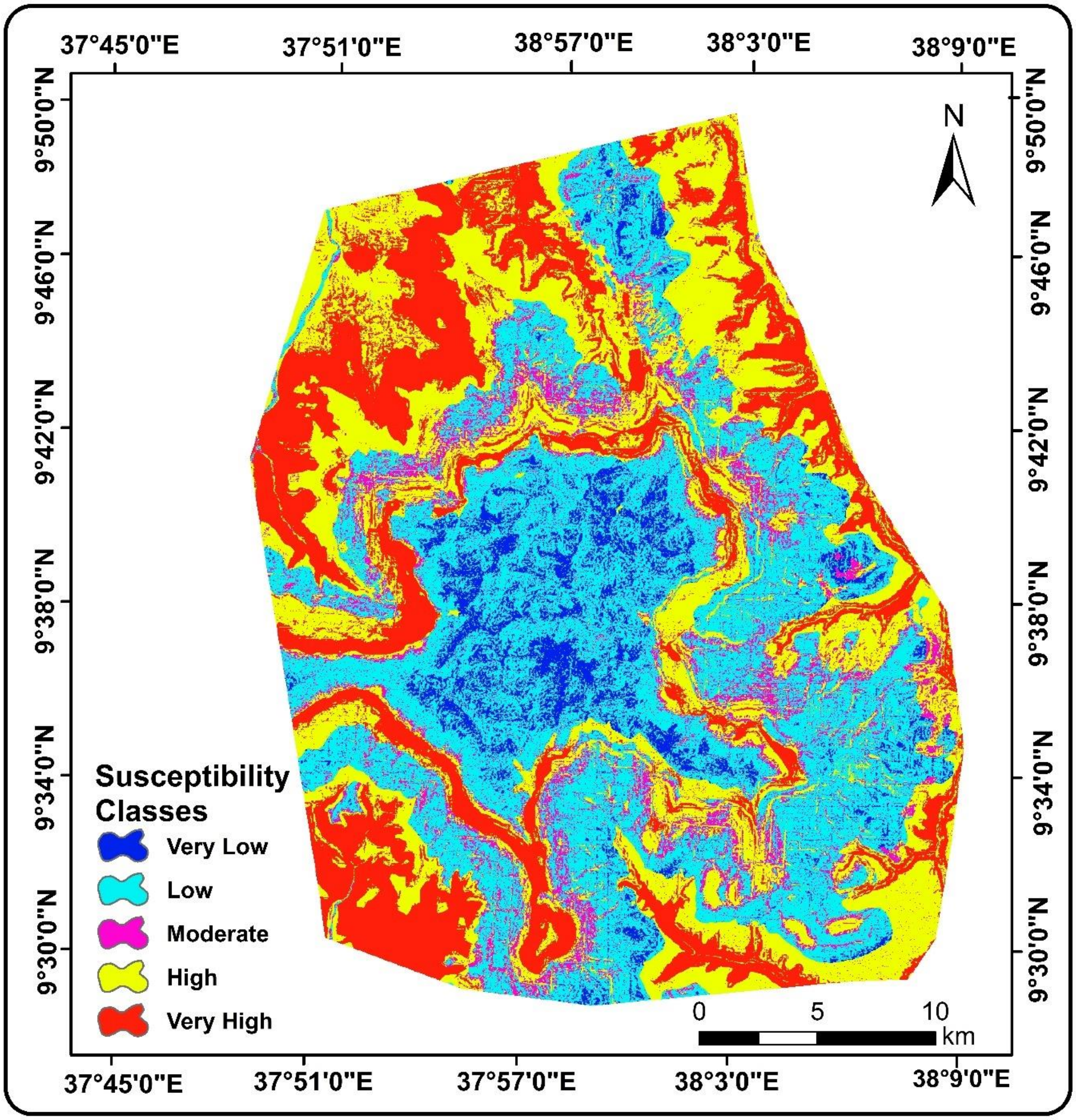

Figure 15 Landslide Susceptibility map using logistic regression

5.6 Verification of the Landslide Susceptibility Maps

In this study, the combination of the landslide susceptibility and landslide inventory map is typically used to determine the quality of a landslide susceptibility model. Out of the 1222 landslides found, 855 (70%) were used to create the landslide susceptibility maps, and 367 (30%) were used to test the model. Both the logistic regression model and the frequency ratio were used to investigate the landslide susceptibility.

For validation, the area under the curves (predictive and success rates) was used by using the 30% validation landslides in both landslide susceptibility maps. The success rate was estimated by comparing the training data set with the landslide susceptibility class, whereas the predictive rate was calculated by comparing the validation data set with landslide susceptibility classes.

5.6.1 Area under the Curve (AUC)

Success and Predictive Rate Curve

The results showed that the AUC of the success rate of frequency ratio and logistic regression models was 0.857 and 0.849, respectively, and the predictive rate of frequency ratio and logistic regression models was 0.828 and 0.831, respectively. The AUC of the success rate and predictive rate curves ranges between 0.8 and 0.9, indicating very good performance of the landslide susceptibility models. Based on the AUC evaluation, the landslide susceptibility maps produced by the models were reliable.

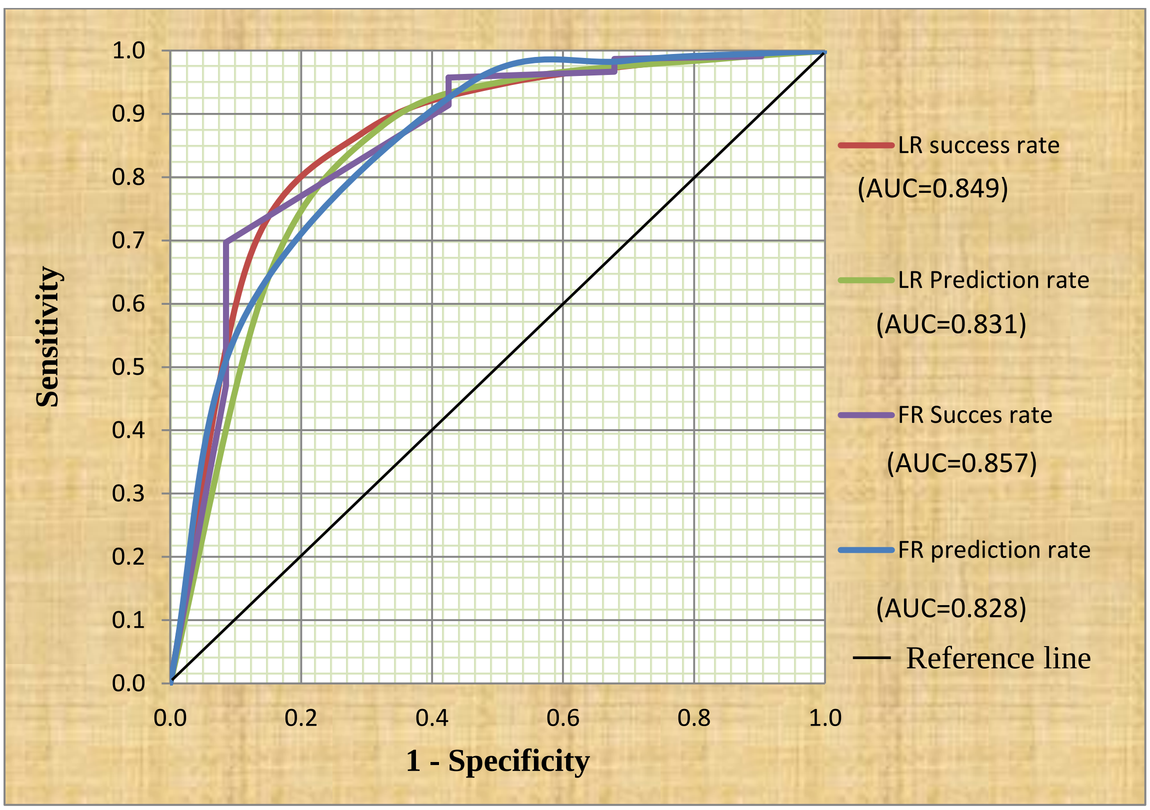

Figure 16 Success and predictive rate of frequency ratio and logistic regression models

6. CONCLUSIONS AND RECOMMENDATIONS

6.1 CONCLUSIONS

Landslide susceptibility assessment is important to assess the probability of future landslide occurrence and can help prepare landslide hazards and risk maps and develop monitoring strategies for landslide-prone areas. In the present study, bivariate statistical-based frequency ratio models and multivariate statistical-based logistic regression models were used to assess the spatial probability of landslide occurrence. Based on the results of the current study, the following conclusions were drawn:

A landslide inventory map was prepared from Google Earth image interpretation in which a total of 1222 landslides were identified that was partitioned in to training (70%) (855) landslides were used in model development, and 30% (367) landslides were used for validation.

In the present study, eight causative factors were considered for preparing the landslide susceptibility maps, including slope, aspect, curvature, lithology, land use/land covers, distance from streams, distance from lineaments, and rain fall. The thematic maps of causative factors, including slope, aspect, and curvature, were prepared from the SRTM DEM with a 30m*30m resolution, and land use land cover and lineament maps were prepared from the Google Earth image of 2023 in ArcGIS environment. The lithological map layer of the study area was extracted from the geological maps of Addis Ababa with a scale of 1:250,000. Rain fall map was generated from the rain-fall data of the National Meteorological Agency of Ethiopia by interpolating in GIS spatial analysis tools, and the stream map was extracted from topo sheets of the study area with a scale of 1:50,000 and mapped in ArcGIS. Later, all vector maps were transformed into raster data for further analysis.

The causative factor maps were combined with a training data set to get each class's weight. Then, the spatial relationship between the occurrence of landslides and each landslide causative factor class was derived. Statistical frequency ratio and logistic regression value were important to identify causative factor classes' contribution to a landslide occurrence. From the frequency ratio analysis, FR values greater than 1 were found in factor class of a slope greater than 14°; concave and convex of curvatures; aspect classes of north, west, southwest and northwest facing slopes; lithology of sandstone and basalt; land use/land cover of shrubs and sparse forest; distance to stream classes between 0 - 500m; distance to lineaments classes of between 0 - 600m that indicated the high probability of landslide occurrence. The remaining FR values of factor classes are less than 1, indicating a lower probability of landslide occurrence. The analysis of logistic regression values of the area where the logistic regression coefficient is positive shows a positive correlation, but if negative, it indicates a negative correlation. The landslide susceptibility index values were divided in to five classes of very low, low, moderate, high, and very high susceptibility by natural break classification method.

AUC values were used to validate the quality provided by the two models, and the resulting landslide susceptibility maps' accuracy was evaluated. In particular, the models' fitting performance and prediction ability have been determined using the validation data set, which is independent landslide data that was not used to build the model and the training set, which is the same landslide data set used to build the model, respectively. Frequency ratio and logistic regression values of success rates of Area under the curve revealed 0.857 and 0.849, respectively, and predictive rates of 0.828 and 0.831 for frequency ratio and logistic regression, respectively. The results of the success rate and predictive rate curves in this study have an AUC between 0.8 and 0.9, indicating that both models performed well and are reliable. The findings and outcomes of this study can aid in predicting future hazard-prone regions for developers, planners, and engineers. The reduction of future damage to infrastructure, properties, the environment, and human life as a result of landslide occurrence will benefit is very important.

6.2 RECOMMENDATION

Based on the findings of the study the following recommendations were forwarded.

- Local administrative must develop appropriate plans to reduce landslide effects through land use and land cover policies and regulations.
- Farming activity carried out near drainage area and on a steep slope greater than 230 should be restricted, and forest conservation activity has to be taken to minimize landslide occurrence.
- The area delineated as very high and high susceptible zones has a probability for future landslide and related slope instability problems. So, before undertaking any

infrastructure development activity in these areas, a detailed study should be conducted.

- The future landslide interventions in Abuna Gindeberet district suggested for land management and concerned bodies should be based on the current study's findings to take more effective management of landslides.

REFERENCE

Addis, A. (2022). *Landslide Susceptibility Mapping Using GIS and Bivariate Statistical Models in Chemoga Watershade , Ethiopia*. 1–21.

Aipe, E., & Sailesh, M. (2016). Landslide vulnerability mapping (LVM) using weighted linear combination (WLC) model through remote sensing and GIS techniques. *Modeling Earth Systems and Environment*, *2*(2), 1–15. https://doi.org/10.1007/s40808-016-0141-7

Aleotti, P.; Chowdhury, R. (1999). Landslide hazard assessment: summary review and new perspectives. *Bull. Int. Assoc. Eng. Geol*, 58, 21–44.

Anis, Z., Wissem, G., Vali, V., Smida, H., & Mohamed Essghaier, G. (2019). GIS-based landslide susceptibility mapping using bivariate statistical methods in North-western Tunisia. *Open Geosciences*, *11*(1), 708–726. https://doi.org/10.1515/geo-2019-0056

Ayalew, L. (1999). The effect of seasonal rainfall on landslides in the highlands of Ethiopia. *Bulletin of Engineering Geology and the Environment*, *58*(1), 9–19. https://doi.org/10.1007/s100640050065

Ayalew, L., Moeller, D., & Reik, G. (2009). Geotechnical aspects and stability of Road cuts in the Blue Nile basin, Ethiopia. *Geotechnical and Geological Engineering*, *27*(6), 713–728. https://doi.org/10.1007/s10706-009-9270-3

Ayalew, L., & Yamagishi, H. (2004). Slope failures in the Blue Nile basin, as seen from landscape evolution perspective. *Geomorphology*, *57*(1–2), 95–116. https://doi.org/10.1016/S0169-555X(03)00085-0

Ayalew, L., & Yamagishi, H. (2005). *The application of GIS-based logistic regression for landslide susceptibility mapping in the Kakuda-Yahiko Mountains , Central Japan*. *65*, 15–31. https://doi.org/10.1016/j.geomorph.2004.06.010

Ayalew, L., Yamagishi, H., & Reik, G. (2004). *Ground cracks in Ethiopian Rift Valley : facts and uncertainties*. *75*, 309–324. https://doi.org/10.1016/j.enggeo.2004.06.018

Ayenew, T., & Barbieri, G. (2005). *Inventory of landslides and susceptibility mapping in the Dessie area , northern Ethiopia*. *77*, 1–15. https://doi.org/10.1016/j.enggeo.2004.07.002

Berhane, G., & Tadesse, K. (2021). Journal of African Earth Sciences Landslide susceptibility zonation mapping using statistical index and landslide susceptibility analysis methods : A case study from Gindeberet district , Oromia Regional State , Central Ethiopia. *Journal of African Earth Sciences*, *180*, 104240. https://doi.org/10.1016/j.jafrearsci.2021.104240

Beza, Y. A. (2021). *GIS-Based Statistical Analysis for Evaluation of Landslide Susceptibility Mapping: A Case Study in Blue Nile Gorge, Gohatsion-Dejen Road Section, Central Ethiopia*.

Broothaerts, N., Kissi, E., Poesen, J., Van Rompaey, A., Getahun, K., Van Ranst, E., & Diels, J. (2012). Spatial patterns, causes and consequences of landslides in the Gilgel Gibe catchment, SW Ethiopia. *Catena*, *97*, 127–136. https://doi.org/10.1016/j.catena.2012.05.011

Carrara, A., Cardinali, M. & Guzzetti, F. (1992). Uncertainty in assessing landslide hazard and risk. *ITCJ*, 2:172–183.

Chandra, S., & Indrajit, P. (2019). GIS - based spatial prediction of landslide susceptibility using frequency ratio model of Lachung River basin , North Sikkim , India. *SN Applied Sciences*, *March*. https://doi.org/10.1007/s42452-019-0422-7

Che, V. B., Kervyn, M., Ernst, G. G. J., Trefois, P., Ayonghe, S., Jacobs, P., Ranst, E. Van, & Suh, C. E. (2011). *Systematic documentation of landslide events in Limbe*. 47–74. https://doi.org/10.1007/s11069-011-9738-3

Corominas, J., & Mavrouli, O. (2023). *Quantitative risk assessmenent for buildings due to rock- falls : some achievements and challenges Quantitative risk assessmenent for buildings due to rock- falls : some achievements and challenges*. *August 2015*.

Cruden, D.M. and Varnes, D. . (1996). Landslide types and processes. In: Turner A.K, Schuster R.L (eds), Landslides investigation and mitigation, Special Report 247, Transportation Research Board,. *National Research Council, Washington, D.C*, 36–75.

Dai, F. C., & Lee, C. F. (2001). *Terrain-based mapping of landslide susceptibility using a geographical information system : a case study*. *923*, 911–923. https://doi.org/10.1139/cgj-38-5-911

Fall, M., Azzam, R.& Noubactep, C. (2006). A multi-method approach to study the stability of natural slopes and landslide susceptibility mapping. *Eng. Geol.*, 82: 241–263.

Faus, T. (2011). Landslide susceptibility assessment: Comparison of Knowledge Based and Data Driven Models. *MSc Thesis, University of Regency, Indonesia.*

Fell, R., Corominas, J., Bonnard, C., Cascini, L., Leroi, E., & Savage, W. Z. (2008). Guidelines for landslide susceptibility , hazard and risk zoning for land use planning. *Engineering Geology*, *102*(3–4), 85–98. https://doi.org/10.1016/j.enggeo.2008.03.022

Genene, A., & Meten, M. (2021). *Landslide Susceptibility Mapping Using GIS-based Information Value and Frequency Ratio Methods in Gindeberet area, West Shewa Zone, Oromia Region, Ethiopia*. http://dx.doi.org/10.21203/rs.3.rs-219331/v1

Getachew, N., & Meten, M. (2021). *Weights of evidence modeling for landslide susceptibility mapping of Kabi-Gebro locality , Gundomeskel area , Central Ethiopia*.

Glade, T. (2003). *Landslide occurrence as a response to land use change : a review of evidence from New Zealand*. *51*, 297–314.

Guzzetti, F., Stark, C. P., & Salvati, P. (2005). Evaluation of flood and landslide risk to the population of Italy. *Environmental Management*, *36*(1), 15–36. https://doi.org/10.1007/s00267-003-0257-1

Hamza, T., & Raghuvanshi, T. K. (2016). GIS based landslide hazard evaluation and zonation – A case from Jeldu District , Central Ethiopia. *Journal of King Saud University - Science*. https://doi.org/10.1016/j.jksus.2016.05.002

Kanungo D.P., Arora, M.K., Sarkar, S. and Gupta, R. . (2009). Landslide susceptibility zonation mapping a review. *J South Asia Disaster Stud*, *2*, 81 – 105.

Kumar, T., Negassa, L., & Kala, P. M. (2015). RESEARCH PAPER GIS based Grid overlay method versus modeling approach – A comparative study for landslide hazard zonation (LHZ) in Meta Robi District of West Showa Zone in Ethiopia. *The Egyptian Journal of Remote Sensing and Space Sciences*, *18*(2), 235–250. https://doi.org/10.1016/j.ejrs.2015.08.001

Lee, S. &Pradhan, B. (2007). Landslide hazard mapping at Selangor, Malaysia using frequency ratio and logistic regression models. *Landslides*, 4:33–41.

Lee, S. (2019). Current and future status of GIS-based landslide susceptibility mapping: a literature review. *Korean Journal of Remote Sensing, 35(1)*, 179–193.

Li, B., Wang, N., & Chen, J. (2021). *GIS-Based Landslide Susceptibility Mapping Using Information , Frequency Ratio , and Artificial Neural Network Methods in Qinghai Province , Northwestern China*. *2021*.

Mandal, S. P. (2018). Comparative evaluation of information value and frequency ratio in landslide susceptibility analysis along national highways of Sikkim Himalaya. *Spatial Information Research*. https://doi.org/10.1007/s41324-017-0160-0

Mersha, T., & Meten, M. (2020). *GIS-based landslide susceptibility mapping and assessment using bivariate statistical methods in Simada area , northwestern*.

Meten, M. (2015). Application of GIS-based fuzzy logic and rock engineering system (RES) approaches for landslide susceptibility mapping in Selelkula area of the Lower Jema River Gorge , Central Ethiopia. *Environmental Earth Sciences*. https://doi.org/10.1007/s12665-015-4377-8

Meten, M., Prakashbhandary, N., & Yatabe, R. (2015). *Effect of Landslide Factor Combinations on the Prediction Accuracy of Landslide Susceptibility Maps in the Blue Nile Gorge of Central Ethiopia*. https://doi.org/10.1186/s40677-015-0016-7

Necdet, T. (2011). *Computers & Geosciences Mapping erosion susceptibility by a multivariate statistical method : A case study from the Ayvalık region , NW Turkey*. *37*, 1515–1524. https://doi.org/10.1016/j.cageo.2010.09.006

Paper, O. (2013). *Landslide susceptibility mapping using GIS-based multi-criteria decision analysis , support vector machines , and logistic regression*. *February*. https://doi.org/10.1007/s10346-013-0391-7

Prakash, N. (2015). *GIS-b based Fr requenc cy Ratio o and L ogistic Regres sion Mode elling fo or Lands slide Su usceptib bility Mapping g of Deb bre Sina Area in Centra al Ethiop*. *12*(2), 1355–1372.

Raghuvanshi, T. K., Ibrahim, J., & Ayalew, D. (2014). Title : Slope stability susceptibility evaluation parameter (SSEP) rating scheme – An approach for landslide hazard zonation. *JOURNAL OF AFRICAN EARTH SCIENCE*. https://doi.org/10.1016/j.jafrearsci.2014.05.004

Rotaru, A., D. O. & P. R. (2007). Analysis of the Landslide Movements. *International Journal of Geology*, *1*(3), 70–79.

Shano, L., Raghuvanshi, T. K., & Meten, M. (2021). *Landslide susceptibility mapping using frequency ratio model : the case of Gamo highland , South Ethiopia*.

Sharma, L. P., Patel, N., & Debnath, P. (2012). *Assessing landslide vulnerability from soil characteristics — a GIS-based analysis*. 789–796. https://doi.org/10.1007/s12517-010-0272-5

Sideng, Uca and Maru, Rosmini and Nyompa, Sukri and Arfan, Amal and Malik, Abdul and Abidin, M. R. (2018). Mapping and Zonation Level of Landslides Hazard and Risk Assessment: A Case Study of Enrekang Regency, South Sulawesi, Indonesia. *Thai Society of Higher Education Institutes on Environment*, 11 (2). pp. 149-163. ISSN ISSN 1906-1714; ONLINE.

Tsige, D., Quezon, T., & Woldearegay, K. (2017). Geotechnical Conditions and Stability Analysis of Landslide Prone Area: A Case Study in Bonga Town, South-Western Ethiopia. *International Journal of Scientific & Engineering Research*, *8*(4). http://www.ijser.org

van Westen, C. J., van Asch, T. W. J., & Soeters, R. (2006). Landslide hazard and risk zonation - Why is it still so difficult? *Bulletin of Engineering Geology and the Environment*, *65*(2), 167–184. https://doi.org/10.1007/s10064-005-0023-0

Woldearegay, K. (2008). Characteristics of a large-scale landslide triggered by heavy rainfall in Tarmaber area, central highlands of Ethiopia. *Geophysical Research Abstract*, *v.10*.

Woldearegay, K. (2013a). *Review of the occurrences and influencing factors of landslides in the highlands of Ethiopia : With implications for infrastructural development*. *5*(1996), 3–31.

Woldearegay, K. (2013b). Review of the occurrences and influencing factors of landslides in the highlands of Ethiopia: With implications for infrastructural development. *Momona Ethiopian Journal of Science*, *5*(1), 3. https://doi.org/10.4314/mejs.v5i1.85329

Wubalem, A. (2021). *Landslide susceptibility mapping using statistical methods in Uatzau catchment area , northwestern Ethiopia*. 1–21.

Wubalem, A., & Meten, M. (2020). Landslide susceptibility mapping using information value and logistic regression models in Goncha Siso Eneses area , northwestern Ethiopia. *SN Applied Sciences*. https://doi.org/10.1007/s42452-020-2563-0

Xu, C., Dai, F., Xu, X., & Lee, Y. H. (2012). GIS-based support vector machine modeling of earthquake-triggered landslide susceptibility in the Jianjiang River watershed, China. *Geomorphology*, *145–146*, 70–80. https://doi.org/10.1016/j.geomorph.2011.12.040

Yalcin, A., & Bulut, Æ. F. (2007). *Landslide susceptibility mapping using GIS and digital photogrammetric techniques : a case study from Ardesen*. 201–226. https://doi.org/10.1007/s11069-006-9030-0

Zerihun.D. (2016). Landslide hazard evaluation and zonation. *MSc Thesis, Addis Ababa University. Addis Ababa.*

APPENDIX

Appendix I Precipitations of six station (31yr); Kachise, Fincha, Shukute, Jeldu, Abay Sheleko and Yejube stations

Stations	Years	month												Annual Rain Fall (mm)
		Jan	Feb	Mar	May	Apr	Jun	Jul	Aug	Sep	Oct	Nov	Dec	
Kachise	1990	7.2	20.4	88.8	34.4	79.7		421.5	481.5	361.9	14.7	0	1	1511.1
	1991	13.7	32.7	96.3	36.4	33.1	246.2	324.3	451.6	239.4	6.5	0.5	17.6	1498.3
	1992	48.4	75.1	52.6	130.4	118.5	292.6	375.8	384.8	222.5	216.8	26.7	8.1	1952.3
	1993	7	36.7	43.7	190.8	282.2	199.5			308.4	98.7	15.4	2.3	1184.7
	1994	7.8	4.2	32.4	62.4	118.1	341.9			176		9	5.1	756.9
	1995	0	7.9	80.6	106.9	204.1	136.8	360.8	250.8	222				1369.9
	1996	34.7		124.3	104.9	218.7	265.2	457.4	312.1	150.5	83.9	35.9	4.4	1792
	1997	30.5		58.3	119.3	148.8	202.6	325.5	301.7	164.2	314.5	180.4	3.1	1848.9
	1998	41.2	0	70.9	8.1	151.5	262.2	290.1	393.8	296.3	202.4	9.2	0	1725.7
	1999	11.1	0	0.9	38.5	105.3	330.7	161.5	552.9	221.1	245.7	7.5	6.8	1682
	2000	0	0	18.5	109.1	114	324.2	340.6	475.8	326.2	143.1	64.3	40.7	1956.5
	2001	0	7	92.7	61.7	123	341.8	387.4	384.2	143.3	92.5	9.6	17.5	1660.7
	2002	60.8	6.6	88.5	52.3	34.3	379.1	209.9	322	148.6	0.9	0	74.9	1377.9
	2003	7.8	17.2	98.2	89	8.4	294.8	512.3	353.8	171.9	39.8	4.1	4.7	1602
	2004	9.5	1.1	135.3	108	38.9	247.8	336.9	495.6	188.3	87.1	8.7	12	1669.2
	2005	18.8	3.9	159	70	127.3	315	478.1	358.3	330	106.4	6.7	0	1973.5
	2006	7.2	27.8	120.7	52.5	121.3	305.7	485.8	426.6	212.8	75.8	43.2	22.7	1902.1
	2007	3.4	37.9	19.3	93.3	146.2	299.8	379.2	406.7	329	52.1	0.8	0	1767.7
	2008	8.3	0.8	9.7	32.9	194.9	457.3	546.9	473.2	254.7	69.3	74	14.7	2136.7
	2009	9.8	8.6	105.3	51	16.5	149.4	357.6	428.2	150.5	97	4.5	15.3	1393.7
	2010	38.9	14.3	113.1	45.8	295.2	341.4	358.4	443.2	258.3	16.9	13.8	8.1	1947.4
	2011	60.9	0.1	95.1	87.5	228.3	218.1	294.6	387.6	270.9	5	112.9	0	1761
	2012	22	0	51.1	66.3	17.4	337.3	396.5	399.5	388.5	35.4	8.8	3.5	1726.3
	2014	15.4	0	24.7	30.5	202	314.8	422.2	378	198.5	202.9	10.9	0	1799.9
	2015	11	4.9	111.8	130.6	318.3	180.7	431.4	391.4	338.1	143.9	62.1	0.93	2125.13
	2016	0.3	5.2	35.8	26.2	347.5	248.6	488.9	463.9	299.1	17.1	66.9	24.6	2024.1

	2017	0	19.7	38.4	112	374.7	271.8	408.9	422.1	266.6		0		1914.2
	2018	0	24.7	41.7	57.9	346.3	242.5	439.5	230.5	258.4	67.7	12.3	0	1721.5
	2019	0.3	0					457	442.1	179.3	83.7	128.3		1290.7
	2020						431			309.6	62		2.2	804.8
	2021			115.2	98.9									214.1
Fincha	1990	6	46.7	73.9	24.2	34.8	357.9	675.8	698.6	557.9		19.2	1.5	2496.5
	1991	0	0	55.4	44	186.1	438.2	622.9	548.6	587.7		0	4.1	2487
	1992	9.2	0	26.8	26.9	75.6	383.1	676.1	635.5	363.1	58.5	41.5	6.3	2302.6
	1993	5.5	8.3	35.6	263.2	96.7		491.1	464.2	275.5	151.1	1.3	0	1792.5
	1994	0	5.5	35.9	56.3	213.4	398.8	392.8	288.2	210	13.8	19.9	6.7	1641.3
	1995	0	29.1	43.3	98.9	199.8	398.9	428	371.5	164.8	18.2	19.1	29.7	1801.3
	1996	20.8	0	5	82.2	312.9		398.4	355.2	303.9	101.8	56.8	12.1	1649.1
	1997	10.2	0	31	128	175.9	285.4	384.8	319	138.2	225.1	24.6	4.2	1726.4
	1998	6.6	12.7	42.6	21.6	225.8	402.3	383.6	360.3	279.3	307.9	14.1	0	2056.8
	1999	18.6	0	5.4	36.9	179.2	396.1	402.2	552.6	353.1	242.1	20.9	30.5	2237.6
	2000	0	0	0.7	93.1	175.1	374.3	290	409.2	374.1	190	43.1	48.6	1998.2
	2001	0	7.3	71.8	109.5	177.2	196.6	417.5	314.7	113.3	167.8	2.8	2.3	1580.8
	2002	33.7	0.5	57.2	130.9	76.4	261.2	360.8	328.5	167.3	8.2	10	37.9	1472.6
	2003	2.8	53.1	81.9	20.1	1.8	466	336.1	307.3	233.5	14.2	15	38.3	1570.1
	2004	7.5	13.2	20.4	68.3	112.4	265.3	382.7	353.3	186.7	140	22.5	0.5	1572.8
	2005	10.5	0	169.8	91	66.1	385.3	339.5	327.4	182.1	114.1	30	0	1715.8
	2006	5	0	71.5	38.8	163.9	359.2		343.7	239.3	61.2	24	56	1362.6
	2007	29	34.4	6	112.4	324.5	305.7	454	366	336.7	14.6	0	0	1983.3
	2008	4.8	0	0	58.2	302.8	306.5	451.1	309.2	183.3	111.9	63.9	0	1791.7
	2009	0	3.1	71.7	37	60.9	413.2	447.7	373.8	181.1	157	11.8	0	1757.3
	2010	34.8	5.1	35.6	110.7	286.7	266.7	475.5	375.8	455.3	33.5	27.9	28.4	2136
	2011	44.8	0	111.2	66.7	247.5	331.6	208.1	226.9	310.7	7.6	47.7	0	1602.8
	2012	0	0	49.5	31.9	63.4	233.6	420.3	382.4	405.7	30	15.7	16	1648.5
	2013	0	0	15.3	1.1	60	233	400.1	303.7	277	110.9	59.9	0	1461
	2014	0	12.8	115.7	160.3	305.3	166.2	263.9	396.9	243.5	214.6	25.9	2.8	1907.9
	2015	0	0	31.2	3	250.5		282	245.2	203.2	4	81		1100.1
	2016	4	12.4	10	16	177	172	309	258	123	19.5	0	1	1101.9

	2017	0	34.5	23.5	69	312.2	194.4	595.2	395.9	293.9	97.2	24.1	0	2039.9
	2018	0					87.9	347.8	315.6	112.1	37.1		0	900.5
	2019					224.6	415.7	727.9		899.7	66.4	47.9	12	2394.2
	2020			42	64.3	347.6	670.1	1287.	547.2	176	94.9	27.6	0	3257.02
	2021	0	2	38.9	125.4	381.2								547.5
Jeldu	1990	8.5	139.1	115.4	46.8	76.1	136.9	355	343.7	233.3	11.5	0.6	3.6	1470.5
	1991	2.2	84.3	168.2	12.3	66.5	243.1	585.2	452.8	677.5	96.4	3	22.2	2413.7
	1992	88.8	97.8	287.4	170.2	180	262	545.3	621.1	465.6	318.5	15.1	11.6	3063.4
	1993		15.4	5.4	514.9	37.1								572.8
	1995		15.4	5.4	515.1	37.1	136.2	249.9	306.9	184.1	14.7	45.8	94	1604.6
	1996	114.4	24.6	166.5	179.9	157.8	264.5	304.5	261.5	169.5	59.4	18.6		1721.2
	1997	47.8	6.6	52.4	92.6	91.7	187.8	225.7	254.6	162.4	124.8	83.6	10.4	1340.4
	1998	47.8	28.8	43.6	58.5	216.4	263.8	232.5	295.1	276.2	76.5	8.8	1.5	1549.5
	1999	48.2	4.7	9.1	23.3	76.8	234	223	236.4	108.6	152.2	11.8	2	1130.1
	2000							224.3	231.4	159.3	68.8	44.3	16.6	744.7
	2001	11.8	25.1	133.7	83.5	163.3	270.7	254.7	216.3	157	64.2	11	31	1422.3
	2002	43.5	41.2	139.7	81.3	74.1	177	269.4	285.9	125.6	18.2	0	17.5	1273.4
	2003	14.7	63.9	80	180.6	3.8	207.7	339.2	465.3	374.5	38.9	0	8.3	1776.9
	2004	0	0	111	132.2	21	176.4	459.4	401.5	199.2	17.6	16.1	7.5	1541.9
	2005	37.9	0.4			112.5								150.8
	2006			156.5		89.9	226	284	360.6			27.7	26.5	1171.2
	2007	29.9		56.2		141.4	260	332.6	214.4	140.7	41.4			1216.6
	2008	3.5			55.6	168							6	233.1
	2009					95.3								95.3
	2010	36	33.9	60.9	70.8		160.4	284.2	139.9	94	8.9	24.9	14.6	928.5
	2011	3.4	1.2	45.6	61.7	76.2	194.3	179	344.2	156.6	5	39.1	0	1106.3
	2012	0	5.7	83.5	72.5	25.6	208.5	310.1	291	103.5	9.1	6.9	7.6	1124
	2014	20.5	4.4	7.1	94.6	117.6	239	261.8	269.4	194.6	69.6	47	0	1325.6
	2015	20.3	38	98	91.1	206.9	88.2	197.8	263.4	214.5	19.4		0.6	1238.2
	2016	0.5	34	39.4	35	119.9	189.1	183.6	198.7	191.8	10.2	49.3	38.8	1090.3
	2017	7.9	51.6	93.2	142.2	155.7	175.6	248	321.4	184.1	63.8	16.5	4.3	1464.3
	2018	0		25.9	33.2	267.2	199.8	277.5	276.5	225.6	54.4		0	1360.1

	2019	3.3					264.1	302.7	274.6	185	36		7.5	1073.2
	2020					157.4			318.2	206.8	42.6	0	3.3	728.3
	2021	2.4	53.6			101.9	130.8	397.1	361.2	163.6	29.3	17.2	23.2	1280.3
Abay sheleko	1990	6.8	20.9	88.9	17.8	49.2	52.5	262.9	269.8	151.4	41.1	0	0	961.3
	1991	0	0	0	0								0	0
	1992		0	11.3	12.1	11.6	17.9	27.2	30.5	20.5	15.2	2	0	148.3
	1993	4.6	0.8	4.9	64.3	100.9	122.7	274.1	184.1	21.5	96.2	0	0	874.1
	1994	0	0	36.1	24.6	137.7	64.8	360.9	272.6	167.6	0	0	0	1064.3
	1995	0	12.3	30.1	73.5	130	122.4	195	235.3	128.3	65	7.4	17.4	1016.7
	1996	4.1	1.5	96.4	129.8	239.9	233	424.3	458.8	135	44.9	56.7	0	1824.4
	1997	65.8	0	111.8	178.5	139.7		354	254.9	92.3	113.5	78.5	14.2	1403.2
	1998	0	2.9	57.4	4.5	80.5	80.1	260.9	326.2	191.2	212.5	0	0	1216.2
	1999	5.2	0	3	16.3	19.7	96.3	372.7	336.4	42.1	165.3	0	6	1063
	2000	0	0	0	64.7	60.1	96.9	296	359	192.7	58.8	39.1	0	1167.3
	2001	0	8.9	38.8	36.4	60.9	222.8	356.1	187.2	60.5	96.8	0	4.1	1072.5
	2002	17.3	0	34.3			172	263.1	254.2	82.1	0	0	17.5	840.5
	2003	0	5.7	26.6	12.8	2.4	183.8	479.3	289.2	351.7	2.1	0	16.1	1369.7
	2004	0	1.7	29.6	30.1	19.1	139.8	239.1	742.1	124.5	48.1	0	0	1374.1
	2005	7.9	0	32.2	0	90.4	105.8	237.4	172.1	328.1	132.4	22.3	0	1128.6
	2006	10.1	8.8	79	64.6	57.8	99.1	365.2	287	206.5	51.2	0	28.4	1257.7
	2007	4.3	73.3	11.3	27.6	145.9	156.8	334.2	300.3	212.2	20.7	0		1286.6
	2008	0	1	0	48.9	150.1	251.1	260.2	220.8	139	50.4	125.9	0	1247.4
	2009	0	0	32.6	59.1	2.3	54.8	328.9	274.4	126.4	128.4	16.6		1023.5
	2010	3.1	2.1	47.7	83.5	115	111.8	168.4	369.4					901
	2011	7.4	0	59.7	27.5	138.9	153.1	220	276.6	187.4	0	162.1	0	1232.7
	2012	0	0	58.5	69.7	33.9	198.5	367.7	348.1	201.8	37.2	8.7	0	1324.1
	2014							215.8	288	223.8	266	5.4	0	999
	2015	0	11.6	0	76.4	117.7	64.5	194.8	233.3	215.3	30.5	27.5	0	971.6
	2016	0	10.5	0	0	163.6	130.5	132.2	268.8	157.4	0	123.3	0	986.3

	2017	0	0	8.2	28.2	97.3	69.5	194.8	203.5	111.4	38.1	0	0	751
	2018	0	13.5	0		145.5	65.6	260.7	255.8	70.6	40.4	0	0	852.1
	2019	0	27.6	3.2	16.2	76.4	313.5	531		225.7	13.5	150.7	0	1357.8
	2020	0	13.7	52	61.9	69	195.2	191	231.1	108.7	0	43.5	17.9	984
	2021	6.8	20.9	88.9	17.8	49.2	52.5	262.9	269.8	151.4	41.1	0	0	961.3
Shukute	2000	0	0	8	63.4	105.6	246.4	421.3	234	191.5	153.5	47.1	12.4	1483.2
	2001		11.7	99.6	127.5	137.2	376.3	417.6	250.3	147	51.9	2.8	17.8	1639.7
	2002	60.7	12.4	143.8	90.9	37.4	235.4	293.8	241.9	128.5	7.8	2	26.9	1281.5
	2003	30	102.8	87.2	155.9	11.5	199.6	386.9	444.7	143.7	8.4	1.6	10.6	1582.9
	2004	0	28	38.1	79.8	47.4	242.5	252.8	300	197.4	20.9	6.5	13.2	1226.6
	2005	88.7	2.6	68.1	79.6	106.9	208.2	271.9	188.5	247.9	26	8.3	0	1296.7
	2006	3.1	20.1	133.4	63.4	119	352.1	504.3	775.5	343.8	42.8	3.8	18.2	2379.5
	2007	20.8	38		31.5	107.2	162.2	711.9	483	394.7	15.2	0		1964.5
	2008					168.3	0	6.6						174.9
	2009	0	6.6	36.5	50.7	54.5						0	18.6	166.9
	2010	0	0	18.9	84	34.3	215.8	349.6	412.9	270.2	165.7			1551.4
	2011			0	53.9	72	162.7	123.4	252.3	396.3	167.9	29.9	122.9	1381.3
	2012	0	0	0	0	0	133.2	290.6	275.7	136.3				835.8
	2014	0	0	151.3	263.5	168.5	213.9	329.3	322.1	146.1	117.6	31.9	0	1744.2
	2015	0	24.6	54.7	173.5	125.8	105.2	322.1	313.6	249.7	34	4	2.6	1409.8
	2016	0	27.6	48.1	36.7	142.9	213.4	206.6	223.7	139.3	0	55.8	27.8	1121.9
	2017	2.4	0	98.1	68.9	305.8	270	283.6	203.4	135.9	35.7	0		1403.8
	2018	0	11.8	6.5	0.4		78.8	396.7	331.9	51.9				878
	2019	8.6	8.8	8	0	25.8	173.6	179.4	154.8	148.6				707.6
	2020	0	3.6	162.4	67.9		132.2	344.7	217.1	93.5	14.2			1035.6
	2021	0	3.6	162.4	67.9		105.7	132.2	344.7	217.1	93.5	14.2		1141.3
Yejube	1990	0	15.4	33.8	82.5	53.3	140.7	316.2	336.9	193.4	33.2	14.4	1.3	1221.1
	1991	8	2.5					407.7	477.6	200.5	3	0	6	1105.3
	1995	6	0	3.5			78.5	202.5	76	77.8	27.6	0	14	485.9
	1996	6	0	19.3	86.4	146.5	119.7	341.3	281.7	131.5	53.2			1185.6
	1997	5.9	0	46.3	149.7	173.8	287.9	332.4	219.5	143.9	148.4	27.1		1534.9

	1998	19.8	5.7	13.6	12	149.6	143.5	261.8	271.4	194	144.6	37.2	0	1253.2
	1999	19.8		0	38.3	44.2	190.5	290.7	272	96.1	171.8	5	2	1130.4
	2000	0	0	0	196.3	57.9	101.1	254.1	321.7	216.6	153.5	34	31.8	1367
	2001	0	0	80.4	0		242.6	317.5	251.8	75.5	63.9	0	5.5	1037.2
	2002	1.5	0	84.3	19.5	26.4	189.8	209	169.8	124.3	0	0	31.1	855.7
	2003	0	36.1	41	23.2	0	202.5	277.1						579.9
	2004		4.3	11.2	71	29		356	346.5	117.9		2.9	2.9	941.7
	2005	3.2	0	120.7	50.9	33.3	324.5	541.6		222.5	82.5	57.8	0	1437
	2006	107	246.1		391.8	346	400.1	48.2	8.9	30.9	1.3	13.9	45	1639.2
	2007	76.4	5.2	5.4	64.9	172.9	166.2	299.5	250.6	215.8	84.8	0.7	0	1342.4
	2008	0	0	0	21	273	365.6	576.3	640.2	448.6	106.4	87.8	0.7	2519.6
	2009	0	14	9.8	46.3	1.7	171.6	446.4	425.3	207.8	96	1.1	15.9	1435.9
	2010	10.1	42.6	37.4	68.4	100.3	102.8	313	382.9	139.2	8.9	0.6	0.3	1206.5
	2011	10.2	0.3	66.1	43.6	105.3	114.5	197.4	470.2	200.8	1.3	41.4	0	1251.1
	2012	0	0	17.5	5.8	12.9	96.3	431.1	408.8		18.7		0	991.1
	2013	0	1.3	13.2	0.8	46.5	211	425	225.8	171.8	69.1	19.7	0	1184.2
	2014	8.3	13.6	26.8	80.1	163.7	149.2	371.9	391.9	242.8	5.5	9.7	0	1463.5
	2015	0	0		33.1	158.9	185.6	196.6	390.5	252.6	19.1	59.5	5.7	1301.6
	2016	0.4	11.7	2.6	28.2	157.9	154.9	157.4	647.6	380.6	113.9	0	0	1655.2
	2017	0	0	14.7	117.9	126.9	403.7	518.3	309.8	148.3	33.4	12.6	0	1685.6
	2018	0	20.2	14.9	113.4	88.2	347.5	448.1	383.8	131.8	88.3	10.3	0	1646.5
	2019	0	1.3	14.1	130.6	157.8	276.8	515.3	406.6	284.6	11	76.6	9.3	1884
	2020	0												0
	2021	0	18.2	0.4	44.6	157	119.2	349.9	643	157.8	99.4	11.8	1	1602.3

APENDEX II Logistic Regression

Variables Entered/Removed[a]

Mode	Variables Entered	Variables Removed	Method
1	Slope LULC Rain fall Aspect Stream Lineament Curvature Lithology		Enter

Model summary

Model	R	R square	Adjusted Square	Std.Error of the Estimate
1	0.401[a]	0.161	0.161	0.23789

a. Predictors: (Constant), slope, LULC, RF, aspect, stream, lineament, curvature, lithology

ANOVA[a]

Model		Sum of squares	df	Mean square	F	Sig.
1	Regression	10840.467	8	1355.058	23944.186	.000[b]
	Residual	56455.538	997582	.057		
	Total	67296.005	997590			

a. Dependent Variable: landslide

b. Predictors: (Constant), slope, LULC, RF, aspect, stream, lineament, curvature, lithology

Collinearity Diagnostics[a]

Model	Dimension	Eigen value	Condition Index	Variance Proportions (Constant)	stream	aspect	curvature	lineament	lithology	lulc	RF	slope
1	1	6.525	1.000	.00	.00	.00	.00	.01	.01	.00	.00	.01
	2	1.000	2.555	.00	.00	.00	.00	.00	.00	1.00	.00	.00
	3	.504	3.598	.00	.01	.01	.00	.04	.11	.00	.01	.47
	4	.364	4.234	.00	.00	.00	.03	.34	.30	.00	.00	.38
	5	.328	4.460	.00	.00	.00	.00	.58	.57	.00	.00	.01
	6	.160	6.384	.00	.01	.02	.93	.01	.00	.00	.01	.13
	7	.062	10.255	.00	.16	.82	.00	.02	.01	.00	.06	.00
	8	.041	12.632	.00	.59	.02	.00	.01	.00	.00	.53	.00
	9	.016	20.192	.99	.24	.13	.03	.00	.01	.00	.39	.00

a. Dependent Variable: landslide

Case Processing Summary

Unweighted Cases[a]		N	Percent
Selected Cases	Included in Analysis	997591	100.0
	Missing Cases	32	.0
	Total	997623	100.0
Unselected Cases		0	.0
Total		997623	100.0

a. If weight is in effect, see the classification table for the total number of cases.

Dependent Variable Encoding

Original Value	Internal Value
non-landslide	0
landslide	1

Block 0: Beginning Block

Iteration History[a,b,c]

Iteration		-2 Log likelihood	Coefficients Constant
Step 0	1	580066.097	-1.709
	2	523469.120	-2.330
	3	520162.835	-2.527
	4	520140.258	-2.545
	5	520140.256	-2.545

a. Constant is included in the model.

b. Initial -2 Log Likelihood: 520140.256

c. Estimation terminated at iteration number 5 because parameter estimates changed by less than .001.

Classification Table[a,b]

Observed			Predicted: Landslide Non-landslide	Predicted: Landslide landslide	Predicted: Percentage Correct	
Step 0	Landslide	Non-landslide	925015	0	100.0	
		Landslide	72576	0	0.0	
	Overall percentage		997590			92.7

a. Constant is included in the model.

b. The cut value is .500

Variables in the Equation

		B	S.E.	Wald	df	Sig.	Exp(B)
Step 0	Constant	-2.545	.004	435938.079	1	.000	.078

Variables not in the Equation

			Score	df	Sig.
Step 0	Variables	stream	4551.569	1	.000
		aspect	4581.714	1	.000
		curvature	23935.600	1	.000
		lineament	51858.309	1	.000
		lithology	61924.354	1	.000
		LULC	128.234	1	.000
		RF	3659.639	1	.000
		slope	119781.270	1	.000
	Overall Statistics		160698.279	8	.000

Block 1: Method = Enter

Iteration History[a,b,c,d]

Iteration		-2 Log likelihood	Coefficients								
			Constant	stream	aspect	curvature	lineament	lithology	lulc	RF	slope
Step 1	1	519250.068	-2.611	.069	.072	.070	.145	.146	.000	.146	.255
	2	418309.998	-4.345	.166	.186	.181	.286	.348	.001	.271	.416
	3	381210.437	-5.312	.153	.217	.266	.369	.461	.256	.166	.425
	4	376608.116	-5.646	.111	.197	.303	.404	.530	.359	.006	.435
	5	376484.564	-5.727	.107	.194	.313	.411	.558	.370	-.034	.440
	6	376484.380	-5.731	.108	.194	.313	.412	.559	.370	-.035	.440
	7	376484.380	-5.731	.108	.194	.313	.412	.559	.370	-.035	.440

a. Method: Enter
b. Constant is included in the model.
c. Initial -2 Log Likelihood: 520140.256
d. Estimation terminated at iteration number 7 because parameter estimates changed by less than .001.

Omnibus Tests of Model Coefficients

		Chi-square	df	Sig.
Step 1	Step	153655.876	8	.000
	Block	153655.876	8	.000
	Model	153655.876	8	.000

Model Summary

Step	-2 Log likelihood	Cox & Snell R Square	Nagelkerke R Square
1	385478.390[a]	.309	.531

a. Estimation terminated at iteration number 7 because parameter estimates changed by less than .001.

Hosmer and Lemeshow Test

Step	Chi-square	df	Sig.
1	26.13	8	.01

Variables in the Equation

		B	S.E.	Wald	df	Sig.	Exp(B)	95% C.I.for EXP(B)	
								Lower	Upper
Step 1[a]	stream	.104	.0099	31.357	1	.000	1.114	1.072	1.156
	aspect	.189	.019	144.806	1	.000	1.214	1.176	1.252
	curvature	.331	.018	1370.389	1	.000	1.367	1.345	1.390
	lineament	.472	.008	10244.156	1	.000	1.509	1.497	1.521
	lithology	.559	.006	8975.759	1	.000	1.749	1.729	1.770
	LULC	.410	.006	19791.947	1	.000	1.448	1.440	1.455
	RF	.370	.023	3.282	1	.070	.965	.929	1.003
	slope	.450	.003	21345.988	1	.000	1.553	1.543	1.562
	Constant	-5.671	.032	31597.183	1	.000	.003		

a. Variable(s) entered on step 1: stream, aspect, curvature, lineament, lithology, LULC, RF, slope.